universität wien

DIPLOMARBEIT / DIPLOMA THESIS

Titel der Diplomarbeit / Title of the Diploma Thesis

"ZrO_2 films deposited by spray pyrolysis from water-based precursor solutions on glass and TCO substrates"

verfasst von / submitted by

Ana Zrilic, BSc

angestrebter akademischer Grad / in partial fulfilment of the requirements for the degree of

Diplom-Ingenieurin (Dipl.-Ing.)

Wien, 2023 / Vienna 2023

Studienkennzahl lt. Studienblatt / degree programme code as it appears on the student record sheet:	UE 066 658
Studienrichtung lt. Studienblatt / degree programme as it appears on the student record sheet:	Masterstudium Chemie und Technologie der Materialien
Betreut von / Supervisor:	Univ.-Prof. Dr. Alexander Bismarck

Abstract

This thesis focuses on gaining a better understanding of depositing stable ZrO_2 layers on transparent conducting oxide substrates while using spray pyrolysis from water-based precursor solutions. $ZrOCl_2 \times 8H_2O$ was chosen – out of curiosity – as the precursor salt for the process. The influence of a range of factors, that play an important role for the spray-pyrolysis process, were studied on three substrates: borosilicate glass, fluorine doped tin oxide (FTO) and tin doped indium oxide (ITO). The precursor concentration was varied between 25mM and 100mM to investigate the behaviour of the ZrO_2 films on the chosen substrates. The scanning repetitions were varied between 75 and 250 to analyse the evolution of crystallisation as the ZrO_2 thickness increased. The temperature of the heating surface was tested between 360°C and 430°C to see its impact on the crystallin character of the films.

The crystal structure, morphology and transmission of the obtained layers were evaluated by scanning electron microscopy, X-ray diffraction and Fourier-transform spectroscopy.

Due to shortcomings it was only partly possible to obtain crystallin ZrO_2 films. Despite the clearly visible formation of cubic zirconium oxide on all samples, the morphological investigation indicates the impact of droplets in its major part, which is not ideal for a vapour phase dependant process. Further optimization of the chosen process and precursor salt is necessary to obtain a successful receipt in order to implement it in further applications such as solar cells or optoelectronic devices.

Contents

Introduction 5

1.1. Structural properties of Zirconium oxide 7

1.2. General procedure of the deposition and critical deposition parameters 8

1.2.1. Influence of the substrate temperature on the film growth by spray-pyrolysis 9

1.2.2. Precursor solutions applied in spray-pyrolysis 10

1.2.3. The precursor salt and solvents used in this work 11

1.2.4. Influence of the pH-value of the precursor solution 12

Experimental 15

2.1. Set-up for the spray pyrolysis deposition 15

2.2. Preparation for the spray-pyrolysis deposition 16

2.3. Precursor solution preparation and experiments 17

2.4. Characterization of the deposited films 17

Results and discussion 19

3.1. Properties of the film deposited on glass substrates 19

3.2. Properties of the films deposited on FTO-coated glass substrates 26

3.3. Properties of the film deposited on ITO-coated glass substrates 36

Introduction

Zirconium oxide (ZrO_2) has a high refractive index, melting point, thermal and mechanical resistance, low thermal conductivity, good oxygen ion conductivity, high dielectric constant and photothermal stability.[1–3] High chemical and photochemical stability with low phonon energy makes it an ideal luminescent host. [4–6] The listed properties of ZrO_2 make it a very interesting material for a wide range of applications, such as solar cells[7], oxygen-conductive membranes (used for fuel cells and electrolysers), optoelectronics, oxygen sensors,[8] or even turbine blades[9] that are exposed to extremely high temperature.

The application of ZrO_2 can also be extended to the field of thin film technology, such as high performance perovskite solar cells (PSC) where zirconia serves as an electron collection / hole blocking layer[10] or in field effect transistors[11] as a gate insulator.

In a number of applications, such as in perovskite cells, the zirconia layer is in direct contact with a thin layer of a transparent conductive oxide (TCO) such as tin doped indium oxide (ITO) or fluorine doped tin oxide (FTO)). It would be thus very advantageous to successfully deposit zirconia on TCOs with a technique that is cost-efficient and compatible with large scale production. Therefore, the focus of this work lies in the preparation of ZrO_2-films on ITO- and FTO-coated glass substrates using spray pyrolysis (SP) - a simple and large-area-compatible deposition method.

Finding a successful recipe for crystalline ZrO_2 deposition could also be expanded to other research fields, where modified zirconium oxide films are of use. For example, Gauckler and Perednis[12] [13]tested fuel cells utilizing thin electrolyte films (of 1 µm) consisting of 8 mol% yttria-stabilized zirconia (YSZ) and a layer of 10 mol% yttria-doped ceria (YDC) solid solution on prefabricated NiO –YSZ anode substrates.

The SP technique can be used for preparing films of various thicknesses but also powders, and ceramic coatings.[14–16] Powders are produced by CVD reactions having a negative free energy change under the used set-up and conditions.[17] Coatings or films are applied by less favorable, preferably endothermic, reactions so that the reaction is predominantly heterogeneous at the surface and gas-phase precipitation is suppressed.[17]

To successfully deposit a thin film on a substrate by spray pyrolysis, we need to optimize the solution composition (precursor salt, solvent, additives, etc) and the spray parameters (solution flow rate, substrate temperature, etc). Multilayers of different films can be easily prepared. Two significant benefits of the spray pyrolysis technique are the simple setup and the cost-

effectiveness of the process. With spray-pyrolysis, materials can be deposited in a thickness range between few nanometers (nm) up to several micrometers (µm).

Various Zr(IV)-based precursor sources[4], such as zirconium(IV) n-propoxide ($Zr[O(CH_2)_2CH_3]_4$), zirconium(IV)-acetate hydroxide ($(CH_3CO_2)_xZr(OH)_y$, x+y ~4), zirconium tetra chlorate ($Zr(ClO_3)_4$), zirconium nitrate ($Zr(NO_3)_4$), zirconium acetylacetonate ($Zr(C_5H_7O_2)_4$ and zirconium oxychloride ($ZrOCl_2 \times 8H_2O$) are known.

However, zirconium acetylacetonate and zirconium oxychloride offer advantages over other precursor salts because no additional additive or chelating agent is needed to stabilize their sensitivity for hydrolysis or pyrolysis.[18]

The deposition conditions have a determining role in the scale-up of the process and on the properties of the coatings. To this end, a very challenging task is to use environment-friendly and non-hazardous solvents for the deposition process, without compromising the quality of the coating. The use of water as solvent can be very advantageous in terms of cost but reports on using water-based solutions for spray-pyrolysis of ZrO_2, as investigated in this work, are very limited.

$ZrOCl_2 \times 8H_2O$ as aqueous precursor salt was reported, but in these reports the spray pyrolysis technique is mainly used for the synthesis of fine particles and not for coatings.[19,20] Some papers describe the deposition of pure zirconia thin films on glass[4,21] or stainless steel[22], but none on transparent conductive oxide substrates, such as FTO or ITO. Deshmuk et al.[4] for example reported the deposition of nanostructured ZrO_2 thin films on glass from a precursor solution containing zirconium oxychloride and (only) double distilled water, which is a rarity in this field. They used the films for the preparation of (ammonia) gas sensors.

The main motivation of this work was to develop a route for the deposition of zirconia thin layers from zirconium oxychloride precursor and water-based solutions, on TCO-coated glass substrates. The reason for this is the upscaling potential and the increased cost-effectiveness of water-based and additive-free processes. The focus lies in the investigation of the effects of the solution concentration, spraying parameters and type of the used substrate, on the morphology, texture, and optical properties of the deposited zirconia films.

1.1.Structural properties of Zirconium oxide

Zirconium oxide exists under atmospheric pressure in three defined crystal structures: monoclinic (m), tetragonal (t) and cubic (c). Each of the three structures is stable in a different temperature regime, as shown in Figure 1.

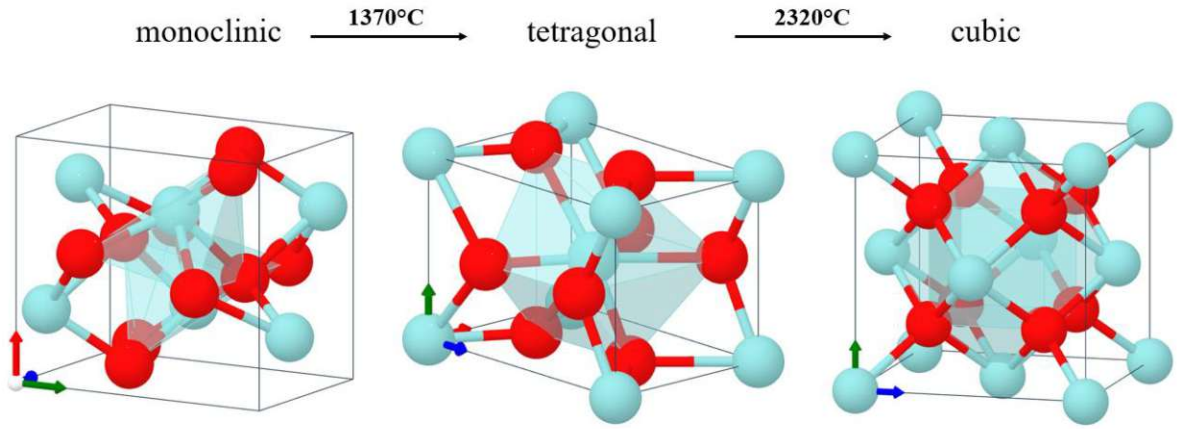

Figure 1: Polymorphic transformation for ZrO_2 and the corresponding space groups: (a) monoclinic ($P2_1/c$), (b) tetragonal ($P4_2/nmc$) and (c) cubic ($Fm\bar{3}m$)[23]

ZrO_2 has a reported wide band gap of ~5.3-6.1 eV[24] (depending on its structure), it is a p-type semiconductor and exhibits abundant oxygen vacancies.[25,26] ZrO_2(m) is considered the thermodynamically stable structure for temperatures below 1370°C, the tetragonal phase is stable in the range between 1370°C-2320°C and the cubic phase at temperatures above 2320°C.[27]

Once the precursor solution passes the nozzle it forms an atomized mist (with droplets of ~10 µm diameter). It can be assumed that three processes take place during the transformation. Firstly, the evaporation of the solvent. Secondly the pyrolytic reaction in which the ZrO_2 is produced and thirdly the crystallization itself. It has been found that amorphous ZrO_2 forms from zirconyl when the process temperature is set to as low as 200°C.[28] When working with spray pyrolysis the reaction temperature can be set high enough so that the ZrO_2 molecules obtain such a high kinetic energy that the crystallisation (the third process) can take place. The cubic phase, which is stable at higher temperatures (HTP), has a simpler structure and higher entropy than the monoclinic low temperature phase (LTP).[29] Since the metastable c-ZrO_2 (HTP) is closer to the amorphous phase it will be formed first during the crystallization stage. Then a transformation from cubic zirconia to t-ZrO_2 or/and m-ZrO_2 could take place depending on the chosen process parameters.

1.2. General procedure of the deposition and critical deposition parameters

The methods of thin-film deposition can be divided in two big subgroups: chemical and physical deposition. The physical methods include laser ablation, molecular beam epitaxy, and sputtering while the chemical methods comprised of gas-phase deposition methods and solution techniques (Fig. 2). The gas-phase methods include chemical vapour deposition (CVD)[30,31] and atomic layer epitaxy (ALE)[32], while solution based techniques, such as spray pyrolysis,[33] sol-gel,[34] spin-[35] and dip-coating[34] methods employ liquid precursor solutions of aqueous or organic origin.

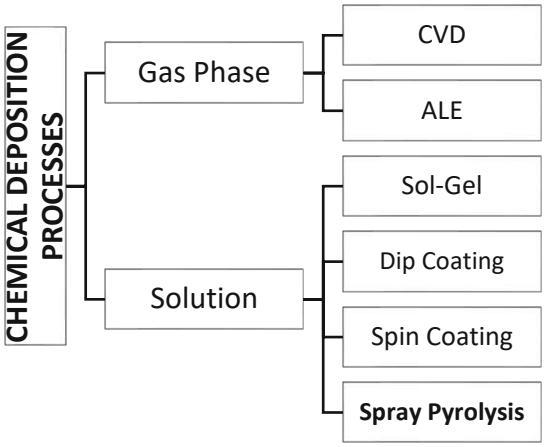

Fig.2: Chemical thin-film deposition methods.

The typical spray pyrolysis set-up consists of an atomizer, precursor solution, substrate heater and a temperature controller. Firstly, the metal-salt precursor solution must be converted into a fine aerosol medium. This is achieved by atomizing the precursor solution. The following atomizers are commonly used in spray pyrolysis techniques: air blast (the liquid is exposed to a stream of air),[36] ultrasonic (ultrasonic frequencies produce the short wavelengths necessary for fine atomization)[37] or electrostatic atomization (the liquid is exposed to a high electric field) takes place.[38]

In this work an ultrasonic generator is used. Ultrasonic atomizers are electrically driven, whereby an electric generator is vibrated at ultrasonic frequencies through a titanium nozzle. Increasing the frequency can result in smaller droplet sizes as shown by equation 1 below.[39] Frequencies of 120 kHz were used for this thesis resulting in an droplet median size of ~10 µm.[40] The formed aerosol is transported to the substrate by a carrier gas where the solvent evaporates, and a pyrolytic reaction and crystallization as described above take place.

The characteristics of the droplets that form within the process are very important for film formation. Lang et al.[41] developed a model that describes the relationship between the droplet

diameter D and the physical properties of a precursor solution, such as the frequency of the ultrasound and the surface tension γ of the precursor. This relationship is described in equation 1:

$$D = 0.34 \left(\frac{8\pi\gamma}{\rho f^2}\right)^{\frac{1}{3}} \quad (1)$$

ρ isthe solution density.

1.2.1. Influence of the substrate temperature on the film growth by spray-pyrolysis

The most important and critical spray parameter is the substrate temperature. The film growth, morphology and properties are most heavily impacted by the temperature to which the substrate and aerosol are exposed. Altering the temperature can, for example, determine the crystal structure of the deposited zirconia film.[11] It is important that the precursor material is transported in the form of droplets to the substrate surface and does not precipitate or form solid particles beforehand, otherwise the requirements for spray pyrolysis are not fulfilled. In this work temperatures between 360°C and 430°C were investigated. Viguié and Spitz[42] described a theoretical process that occurs in spray pyrolysis when the material is transported from the nozzle to the heated surface with increasing substrate temperature.

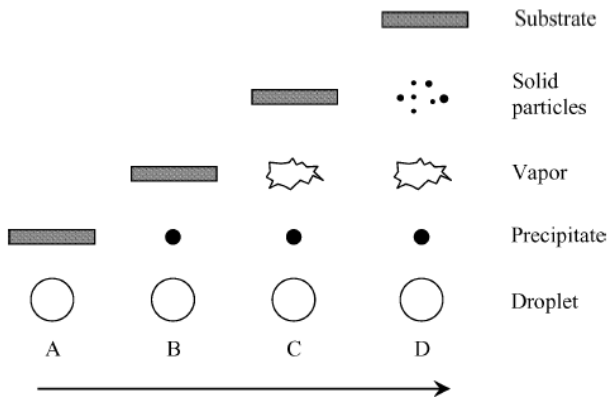

Figure 3: Precursor deposition processes initiated with increasing substrate temperature.[42]

If the temperature to which the atomized precursor solution is exposed is too low, the droplet splashes onto the substrate surface, vaporizes, and leaves a dry precipitate in which decomposition can occur (process A). If the material is exposed to higher temperatures than in process A, the solvent evaporates before reaching the surface and the material precipitates. Subsequently, the precipitate hits the substrate, where it decomposes (process B). If the solvent evaporates, earlier than in process B the so-formed precipitate melts and vaporizes. The vaporized material diffuses to the substrate and undergoes a

CVD-like process (process C) (CVD: chemical vapor deposition). The temperature at which process C occurs is regarded as the optimal deposition temperature. If the system is exposed to a temperature that would be considered too high for the chosen material, the precursor vaporizes too early and solid particles are formed during a chemical reaction in the vapour phase (process D). A non-adherent solidification is the result. All other process types, A, B and C lead to the formation of an adherent film.

1.2.2. Precursor solutions applied in spray-pyrolysis

Together with the temperature, the composition of the precursor solution is the most important process factor. The chemical and physical properties of the precursor solution are defined by the solvent, type of salt, additives, and their concentration. Often the solutions are modified with additives to improve or alter the properties of the produced film or powder.

Cho et al.[43] for example prepared ZrO_2 powders by ultrasonic spray pyrolysis using $ZrOCl_2 \times 8H_2O$ as the precursor salt and distilled water as solvent. By adding H_2O_2 (10% to the total precursor solution volume) the morphology of the zirconia powder improved. ZrO_2 powder prepared by using only zirconylchloride contained many "shell fragments", (term used by the author to describe a non-homogenous, rough surface) while the ZrO_2 powder prepared by using $ZrOCl_2 \times 8H_2O + H_2O_2$ exhibited no shell fragments, forming a smoother film.[43]

But additives can also be used to dope zirconia. Habubi et al.[44] prepared nanostructured ZrO_2 thin films doped with Cu (1% and 3%) by spray pyrolysis deposition. The precursor solution had a concentration of 0.1M $ZrOCl_2 \times 8H_2O$ and $CuCl_2 \times 2H_2O$ was used as the doping agent. Results showed that the crystallite size becomes bigger after the doping. Properties such as the transmittance, bandgap energy and absorption coefficient decreased with increasing dopant content.[44] Other films deposited by spray pyrolysis and doped with doping agents containing praesidium, europium and terbium were shown to be photoluminescent when prepared with $ZrOCl_2$ based precursor solutions.[45–48]

Also, polymer additives can be added to the precursor solution. Perednis et al.[49] investigated the effect of adding polyethylene glycol (PEG) to the precursor solution for depositing yttrium-stabilized zirconia (YSZ) thin films on nickel alloy substrates. Depending on the desired stoichiometry, the aqueous precursor solution consisted of a mixture of zirconyl and yittrium nitrate. The obtained films showed cracks on the surface. Modifying the properties of the precursor solution by adding polyethylene glycol (PEG; 6000 g/mol), the morphology of the film changed from cracked to crack-free.[49] This was explained by the authors with the binding

properties of the polymer. The lower surface roughness suggested that the polymer improved the spreading behaviour of the droplets on the substrate.

So, adding additives remains a very common practice for solutions used in spray pyrolysis as a leverage to control the morphology and properties of the deposit. Nevertheless, a very challenging task is the deposition from water-based precursor solutions, which would increase the upscaling potential and cost-effectiveness. A high amount of energy is required so that precursor salts in water-based solutions can undergo thermal decomposition. Water has a high surface tension and as shown in equation 1 high surface tension leads to formation of larger droplets. Smaller droplets lead to a faster evaporation because of the increased droplet pressure, which can be taken advantage of in the spray pyrolysis process. The strong hydrogen bonds that water molecules form when in liquid state are the reason for the high surface tension (72.8 mN/m at 20°C) and relatively high evaporation temperature of water.[50] The temperature has to be high enough to break the hydrogen bonds but cannot be too high due to process limitations. This makes the determination of the optimal deposition temperature a difficult task. However, the use of water as solvent has advantages in terms of process cost and required safety measures for industrial production (compared to the use of flammable organic solvents).

Reports on water-based solutions via spray pyrolysis for depositing ZrO_2 thin films are very limited. Organic solvents, such as methanol (22.5 mN/m at 20°C), have a lower surface tension and, therefore, require less energy to reach their boiling point and transform the precursor solution into a stable oxide film.[51] As shown in equation 1 the droplet size is highly dependent on the surface tension and would therefore result in tighter droplet size distribution for organic solvents.[40] However, avoiding them is in general of big interest, due to the environmental impact and safety risks that come with the usage of the process at high temperatures and toxic or flammable solvents.

1.2.3. The precursor salt and solvents used in this work

In order to form a stable ZrO_2 film, zirconium needs to be stabilized in its oxidation state (IV) in the precursor solution. Zirconium ions show a strong tendency towards hydrolysis and polymerisation when the concentration of the Zr^{4+} solution is greater than 10^{-4}M. When the ions are exposed to an aqueous medium the so called tetrameric (solution) species $[Zr_4(OH)_8(H_2O)_{16}]^{8+}$ is formed.[22,52,53]

Stabilization of ionic species is important for solutions that are used for chemical depositions. The prior mentioned tetranuclear complex can be stabilized in acidic aqueous solutions, to prevent precipitation of ZrO_2.

The main subject of this thesis is to investigate the deposition of zirconium oxide layers using Zirconium (IV) oxychloride octahydrate **$ZrOCl_2 \times 8H_2O$** as the precursor salt.

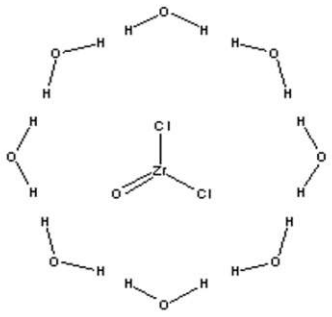

Fig. 4: Chemical structure of $ZrOCl_2 \times 8H_2O$

Muha and Vaughan[54] have established that $ZrOCl_2 \times 8H_2O$ exists in the form of the complex salt and adopts a tetrameric structure of $[Zr_4(OH)_8]Cl_8$, featuring four pairs of Zr^{4+} centres when diluted, whereby the Zr^{4+}, being a strong Lewis acid contributes to the acidic character of the solvent.[55] Water-based solutions using zirconyl chloride to deposit ZrO_2 have been reported, but mainly for application on metals or steel.[56,57]

Since a future research goal would be to build thin film photovoltaic devices incorporating ZrO_2, the following substrates were used: (a) fluorine-doped tin oxide (FTO)-coated glass, (b) tin-doped indium oxide (ITO)-coated glass and (c) plain borosilicate glass. The FTO and ITO, as transparent conductive oxides (TCOs), provide high transparency and low sheet resistance, both important requirements for use in photovoltaic or optoelectronic devices.

1.2.4. Influence of the pH on the precursor solution

The pH of the precursor solution defines the ions and complexes that are stable in solution. It therefore impacts grain growth and stoichiometry of the film. Depending on the used precursor salt and its chemical properties, the salt can influence the solution by contributing to an acidic or basic character when diluted with the solvent and thus alter the pH-value.

In spray pyrolysis deposition acids are often used to regulate the solution pH. The use of acetic acid for example is known to increase the stabilization of organic-metallic precursors in water, however a value that is too low can influence the growth rate negatively. Speciation diagrams are useful in determining the distribution of species in the solution for different pH values.

In Figure 5 the speciation diagram for Zr^{4+} is presented. The concentration of the Zr(IV) species was set to 100 mM as used in the experiments with zirconium oxychloride. The diagram was created using the software MEDUSA (Make Equilibrium Diagrams Using Sophisticated

Algorithms) and the associated database HYDRA (Hydrochemical Equilibrium Constant Database).

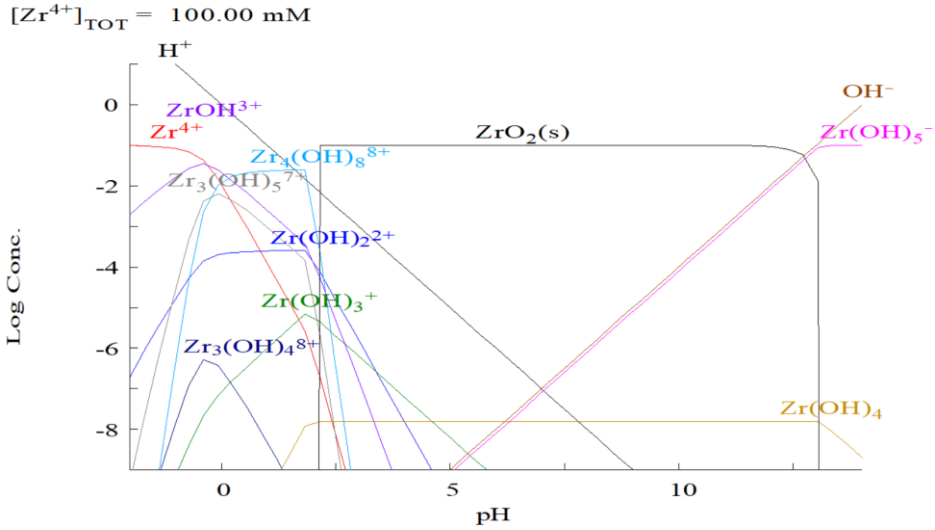

Figure 5: Speciation diagram for the Zr^{4+} - H_2O system

The speciation diagram is plotted in terms of the logarithms of the concentrations of the ionic and polynuclear species as a function of the pH of the solution.[58] The curve for Zr^{4+} in Fig. 5 shows that the concentration decreases rapidly, with increasing pH and zeros at a pH of ~2.8. For pH values higher than 2.0 solid ZrO_2 precipitates. The diagram also shows that Zr^{4+}-ions are relatively unstable and attract hydroxyl groups under acidic conditions, making $[Zr_4(OH)_8]^{8+}$ the dominant species in the pH range 1≥ pH ≤3. The values for the equilibrium constants logK of the hydroxide species that were used from the HYDRA database to create the speciation diagram are displayed in Table 1.

Complex species	*log K (25°C)*
$[OH^-]$	-14
$[Zr(OH)_2]^{2+}$	-1.7
$[Zr(OH)_3]^{+}$	-5.1
$[Zr(OH)_4]^{0}$	-9.7
$[Zr(OH)_5]^{-}$	-16
$[Zr_3(OH)_4]^{8+}$	-0.6
$[Zr_3(OH)_5]^{7+}$	3.7
$[Zr_4(OH)_8]^{8+}$	6
$[Zr(OH)_3]^{+}$	0.3

Table 1: Complex stability constants for the hydrolysis species of Zr^{4+}.

The formation of an aqueous species is based on its equilibrium constant K^0, which is also known as the hydrolysis constant K_h for aqueous systems. The values of the hydrolysis constant are used to determine the speciation diagram of each ion and complexes that are stable in the solution.

The equilibrium constant K_h is related to the Gibbs standard free energies of reactions (ΔG_r^0):

$$\Delta G_r^0 = -RTlnK_h \qquad (2)$$

The discussion in this work is concentrated on samples that were deposited from $ZrOCl_2 \times 8H_2O$ aqueous solutions. When zirconyl is diluted in pure water to form a 0.1 M solution the pH of the precursor solution is as acidic as 1.24 because Zr(IV) has a low electron ionization potential, making it a strong Lewis acid.

Experimental

2.1. Set-up for spray pyrolysis deposition

The used set up, experimentation equipment, sample preparation and precursor preparation protocols are presented in the following.

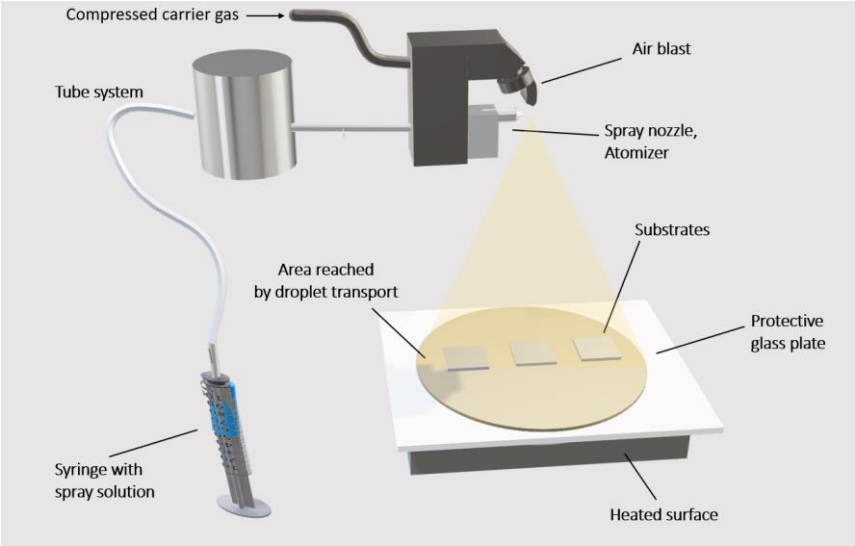

Figure 6: Simplified set-up of the spray pyrolysis process.

The spray pyrolysis was carried out using a Sono-Tek Exacta Coat® system, with a 120 kHz Sono-Tek Impact® ultrasonic nozzle in the horizontal geometry, situated 20 cm above the heated substrates. The scanning speed of the nozzle over the substrate was 25 mm s^{-1}. The high-temperature hot plate of the spraying system was covered by a 20×20 cm^2 glass plate for protection in order to achieve a homogeneous heat distribution. The hot plate can be heated to temperatures up to 600°C. The precursor solution filled the syringe and was pumped through the tube system to the spray nozzle at a defined and constant flow rate. The solution flow rate was kept at 0.8 ml min^{-1} and compressed air with 0.5 bar overpressure was used as shaping gas for the aerosol plume. The process was done using several spraying cycles ranging from 75 to 250 repetitions.

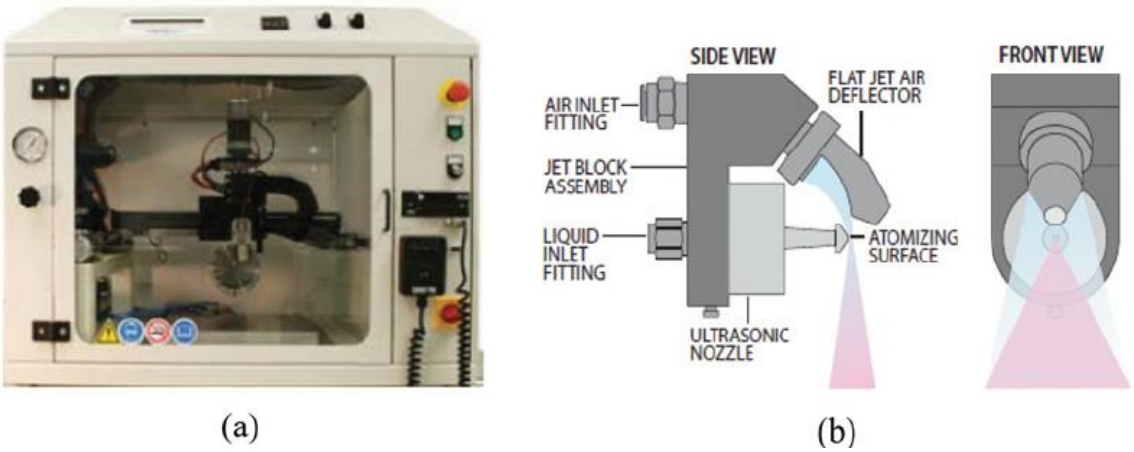

Figure 7: a) Exacta Coat Lab Scale equipment for producing thin films b) schematic of the ultrasonic atomizer.

2.2. Preparation for the spray-pyrolysis deposition

Borosilicate glass substrates (Schott Nexterion® D, 7.5 × 2.5 cm^2) and pure SiO_2 substrates (Plan Optik, 2.5 × 2.5 cm^2) were ultrasonically cleaned for 30 min at 50°C in Hellmanex® III washing solution. The substrates were afterwards rinsed with deionized water (DI, 18 MΩ cm^{-1}), isopropanol and dried in a nitrogen stream. Commercial tin-doped indium oxide (ITO, Sigma-Aldrich 703192, 8–12 Ω Sq^{-1}) and fluorine-doped tin oxide (FTO, Sigma-Aldrich 735140-5EA, 5–7 Ω Sq^{-1}) glass substrates were rinsed twice with isopropanol and dried in a nitrogen stream.

All substrates were placed on the 20×20 cm^2 glass plate before the heating plate was turned on. The hot plate of the SONO TEC® was then set to the target temperature between 310°C and 430°C. The SONO TEC® tube system was first cleaned with 25 mL of pure double distilled water (before the heating plate was turned on) and once again after the working temperature was reached. The solutions were pressed through the system with a Hamilton 50 mL syringe until the tubes were empty. After cleaning the machine, the Hamilton syringe was filled with the precursor solution, of which 25 mL were pressed through to wet the tube system. Afterwards the syringe was filled with the remaining precursor solution and the spray pyrolysis started.

After the deposition, the system was cleaned two times with double distilled water and air was pressed through the system. The samples were cooled down for 30 min and investigated via a scanning electron microscopy, X-ray diffraction and Fourier transform VIS-NIR spectroscopy.

2.3. Precursor solution preparation and experiments

Fresh precursor solutions with a volume of 100 mL were prepared for each deposition run. 3.8 g of pure zirconyl chloride ($ZrOCl_2 \times 8H_2O$, Sigma Aldrich 7699-43-6) was diluted in 100 mL double distilled water to obtain solutions of 0.1 M. Furthermore, 1.61 g of zirconyl chloride were diluted for the 0.05 M and 0.81 g for the 0.025M concentrated solution.

In order to homogenize and completely dissolve the prepared precursor solutions, they were afterwards placed in an ultrasonic bath for 30 min at room temperature. Afterwards the pH of the solutions was measured with a pH/ion meter (Mettler Toledo SevenCompact S220).
$ZrOCl_2 \times 8H_2O$ - salt precursor solutions with a concentration of 0.025 M (pH = 1,14), 0.05 M (pH = 1.20) and 0.1 M (pH = 1.24) were used. The scan rate was set to 0.8 ml min^{-1} for all conducted experiments.

Three different sets of experiments were conducted. In the first one the precursor concentration in the solution varied from 25 mM to 100 mM while the scan number was kept constant at 200 scans and the temperature at 380°C. In the second set of experiments, the precursor concentration was kept constant at 100 mM, while the scan was increased from 75 to 250. In the third set of experiments the deposition temperature was varied between 360°C and 430°C, while the precursor concentration was kept at 100 mM and the scan number at 250.

2.4. Characterization of the deposited films

Morphology

A Zeiss SUPRA 40 **Scanning Electron Microscopy (SEM)** was used to investigate the morphology of the deposited zirconia films. Top-view and cross-sectional micrographs were taken and are discussed in the following chapter. Acceleration voltage was set to values ranging from 3kV to 5kV. The images were acquired with an in-lens detector. Because of the conductive properties of both FTO and ITO, additionally coating was not necessary to investigate the ZrO_2 layers onto them. The deposits created on the borosilicate glass substrates were not analysed with SEM, due to its insulating properties. Sputter-coating the glass samples with an electrically conducted metal was not carried out.

Crystal structure

The crystal structure of the deposited films was analysed with an **X-ray diffractometer (XRD)** (ThermoFisher Scientific ARL Equinox 100) at an angle of 5 °, using Cu-K_α (l = 1.5419 Å) radiation. The Crystalllography Open Database (COD)[59] was used for the Joint Committee on

Powder Diffraction Standards (JCPDS) standards of the metal oxides and the software Match! for the analysis of the diffractograms.

Transmission

VIS – NIR transmittance spectra were recorded in the spectral range between 300 and 1100 nm with a **Fourier-transform VIS-NIR spectrometer (FT-S,** Bruker Vertex 70). In order to cover the visible spectrum a Gallium-Phospide (GaP, covering 303 – 550 nm) detector and a Silicon (Si, covering 550nm – 1150 nm) detector were used.

Results and discussion

According to the phase diagram of ZrO_2/Y_2O_3, at an Y_2O_3 content of 0% the stable phase for zirconia below 1500°C is m-ZrO_2.[60] Zirconium oxide transforms as the temperature increases by martensitic transformation to the other two polymorphic phases: tetragonal (1373 K to 2173 K) and cubic (above 2173 K).[61] In the present work the appearance of the cubic metastable phase was observed at room temperature whilst measuring XRD diffractograms. The occurrence of a high temperature phase (HTP) at low temperatures can be linked to kinetic peculiarities of the process when the precursor solution transforms into an oxide. This effect was discussed by Xiaming et al.[28] while studying the phase formation of ZrO_2 and ZrO_2-Y_2O_3 powders from aqueous solutions of $ZrOCl_2 \times 8H_2O$ and $Y(NO_3)_3 \times 6H_2O$.

For all depositions the ZrO_2 peaks match well with cubic ZrO_2 (COD-ID: 96-210-2135). As mentioned before, in the present work, two types of TCO-coated glass substrates were used: one coated with FTO and the other with ITO. The third substrate that was used is bare borosilicate glass.

3.1. Properties of the film deposited on glass substrates

Deposits created with different precursor solution concentration

In a first set of experiments, the number of scanning repetitions was set to 200 and the deposition temperature was held constant at 380°C for all experiments, leaving the solution concentration the variable parameter. The X-ray diffractograms of the ZrO_2 films deposited on bare glass substrates, with different concentrations, are shown in Figure 8. Also shown is the diffractogram of the bare glass (without deposited ZrO_2) and the standards for cubic ZrO_2.

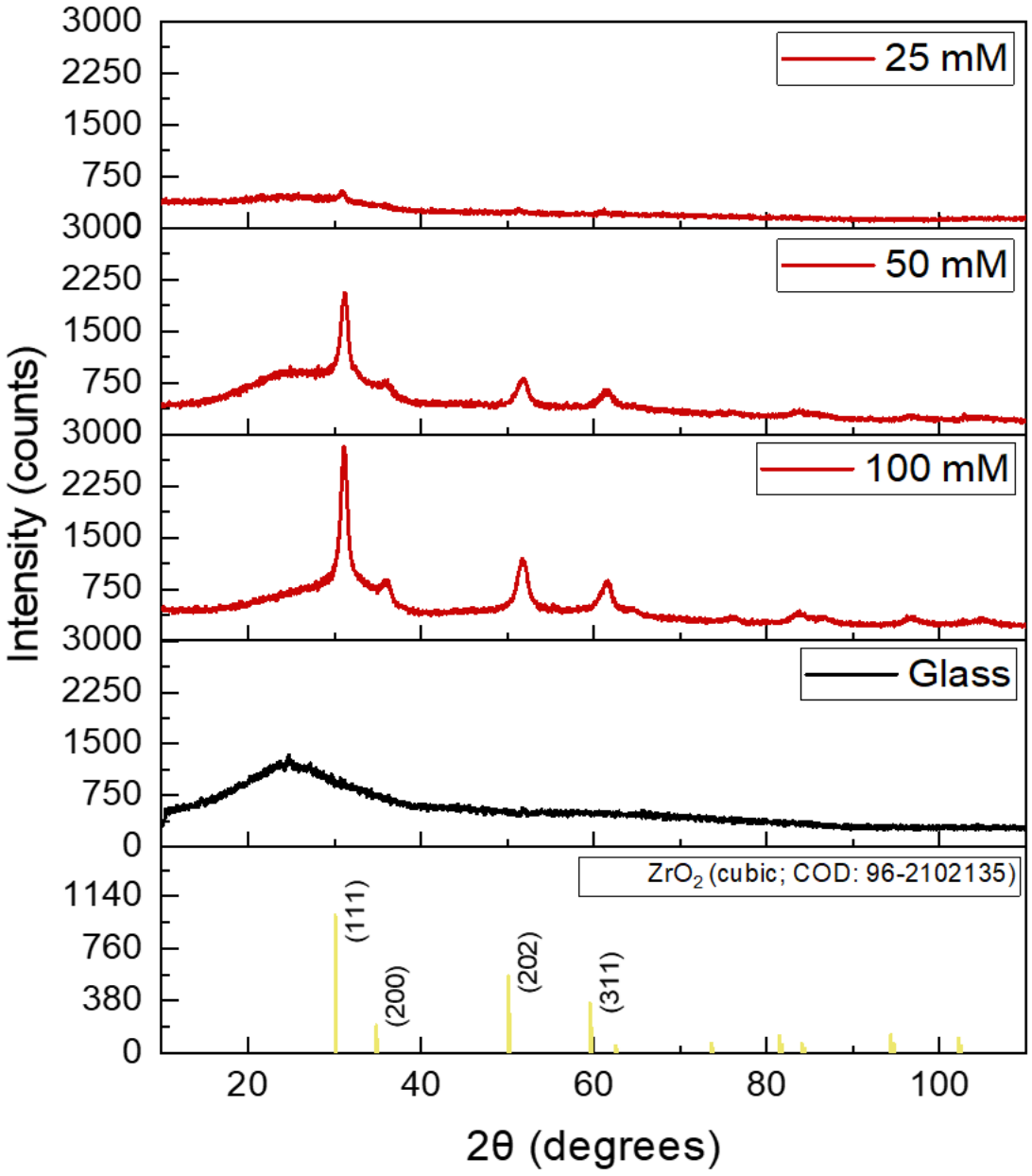

Figure 8: X-ray diffraction patterns of cubic ZrO_2 films, sprayed onto a substrate with a T=380°C at 200 scanning repetitions with varying solution concentration of 25, 50 and 100 mM on borosilicate glass, along with the diffractogram for the bare glass substrate and the JCPDS standard for cubic ZrO_2.

The deposited films have a pronounced cubic ZrO_2 (111) texture. The (202), (311), (200) peaks have a lower intensity but are clearly visible for the films deposited from solutions with a concentration of 50 and 100 mM. The intensity of the peaks increases with increasing solution concentration, which is predominantly linked to the increase of the film thickness. For the 25 mM case only the major (111) peak can be distinguished. The broad background originates from the glass substrate with a possible contribution from an amorphous phase of the ZrO_2 deposit.

The optical transmission spectra measured borosilicate glass coated with ZrO_2 from solutions with varying concentration (Fig. 9), prove the same, where the increase of concentration leads to a reduction of the transmittance, which is linked to the increase of the film thickness. With a precursor concentration

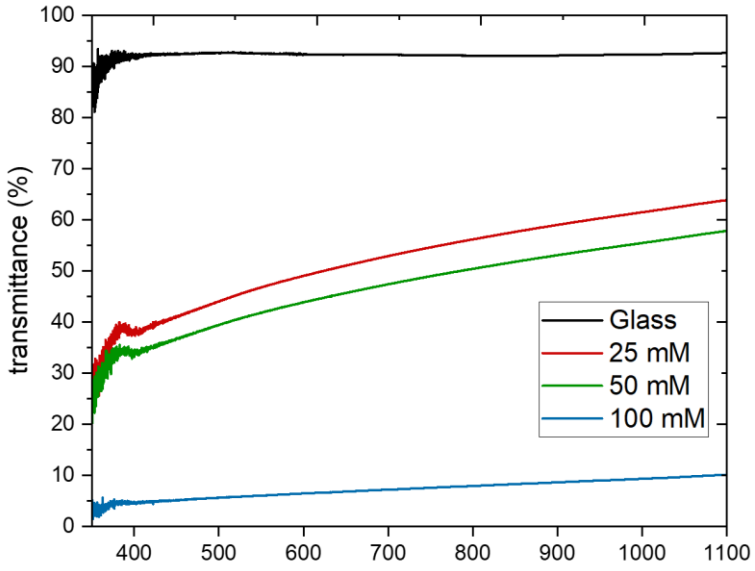

Figure 9: Optical transmission spectra of the cubic ZrO_2 films, sprayed at T=380°C and 200 scanning repetitions with varying solution concentration of 25, 50 and 100 mM on borosilicate glass.

Deposition with varying scan number

In the second set of experiments, the deposition temperature and concentration were held constant at 410°C and 100 mM. It is noted that the temperature was somewhat increased compared to the previous set of depositions, as we have observed a better film crystallization at the increased temperature. The scan number was varied from 75 to 250. The target was to investigate the evolution of crystallization as the ZrO_2 thickness increased. The X-ray diffractograms are shown in Figure 10.

It can be seen that (111)-textured c-ZrO_2 films are obtained even for 75 scans. The texturing becomes more pronounced with increasing film thickness and is therefore the most pronounced for 250 scans.

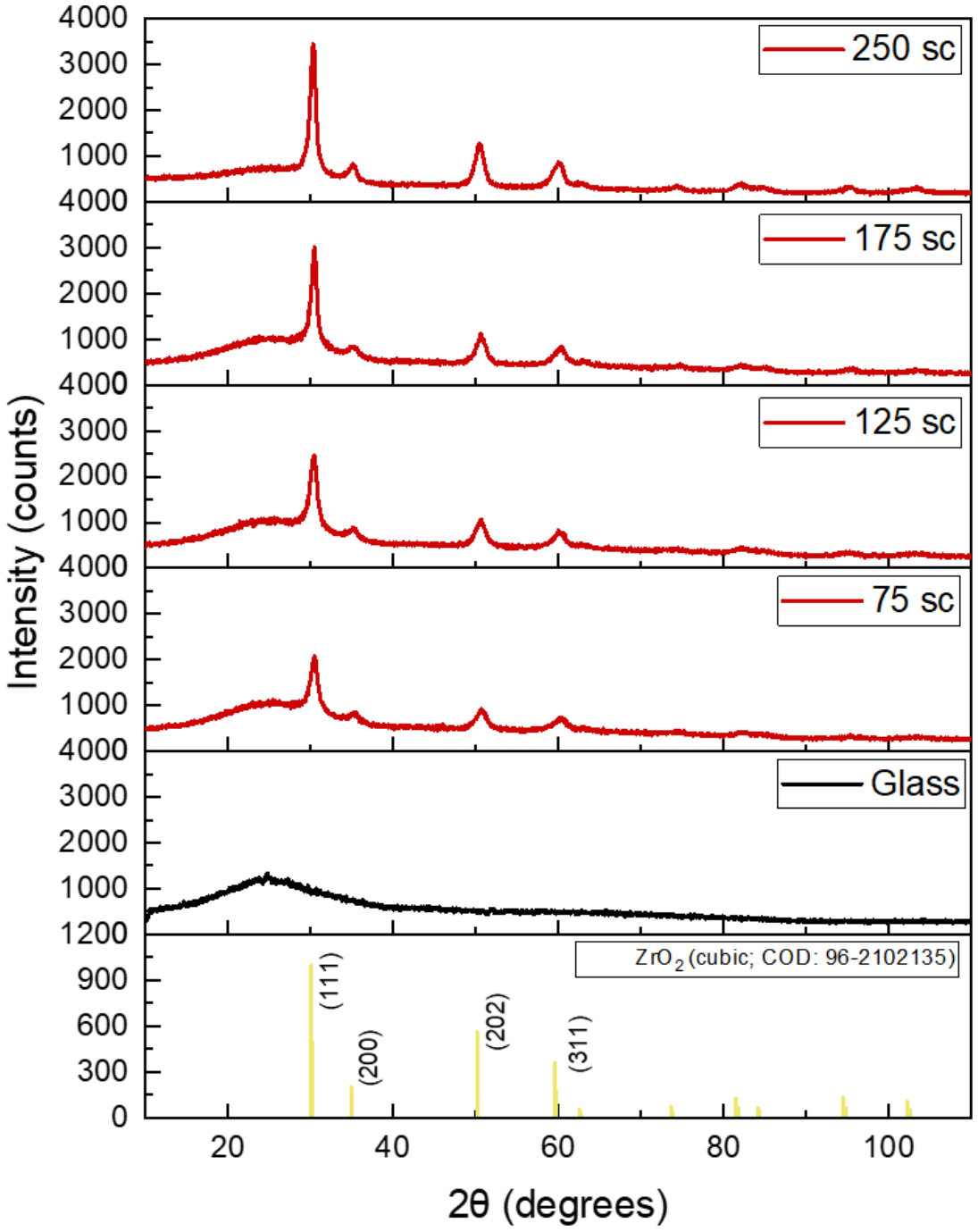

Figure 10: X-ray diffraction patterns of ZrO_2, sprayed at T=410°C and c=100 mM on borosilicate glass with scanning number ranging from 75 to 250 scans (sc). Also shown is the diffractogram of the glass substrate and the JCPDS standard for cubic ZrO_2.

In Figure 11, the transmission spectra of the glass substrate and the deposited zirconium oxide layers indicates an increased coverage of the sample with increasing scan number, which goes hand in hand with the according XRD-graphs presented in Figure 10.

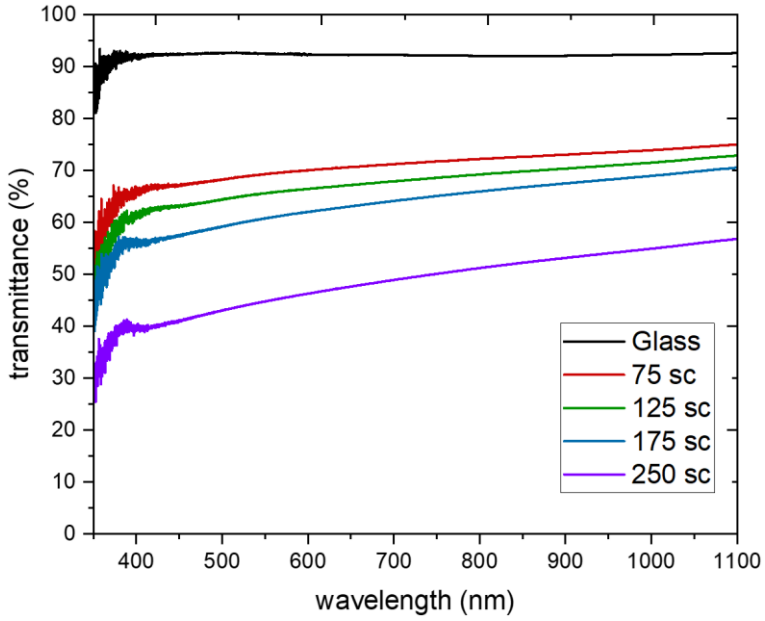

Figure 11: Optical transmission spectra of the cubic ZrO_2 films sprayed at T=410°C and c=100 mM on borosilicate glass with scanning number ranging from 75 to 250 scans (sc).).

Depositions with varying temperature

In the last set of experiments, the number of scanning repetitions was set to 250 and the concentration to 100 mM leaving the temperature the only variable parameter. Temperatures of 360, 410 and 430°C were investigated. The X-ray diffractograms are shown in Figure 12. The film deposited at the lowest temperature of 360°C had the lowest intensity peaks, with the most prominent peak being the (111) and a broad background visible as described in the previous experiments. With increasing temperature the ZrO_2 (200), (202) and (311) peaks gained in intensity. However, the peaks with the highest intensities are obtained for the deposition at 410°C.

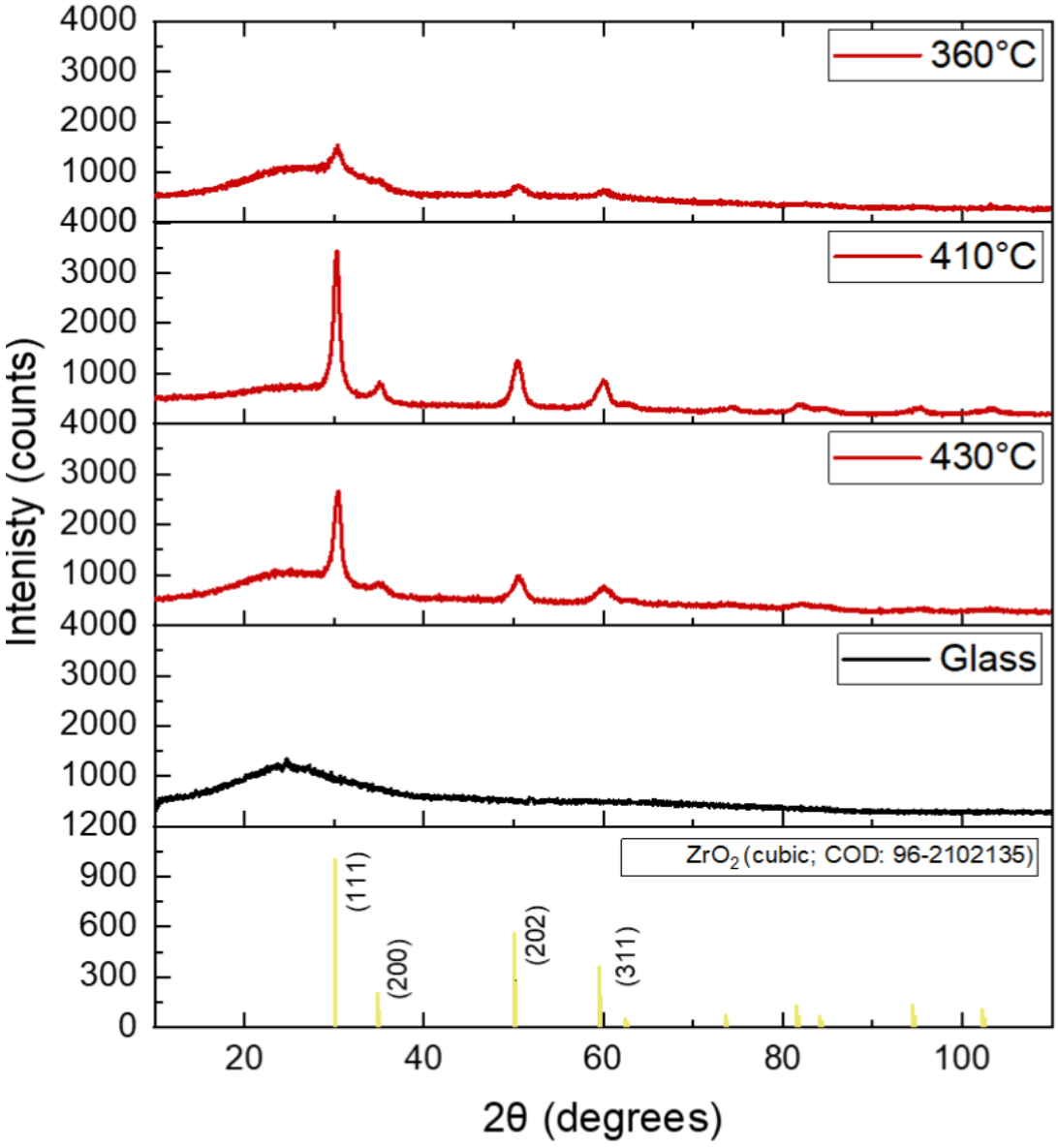

Figure 12: X-ray diffraction patterns of the cubic ZrO_2 films, sprayed at temperatures between 360°C and 430°C on borosilicate glass, along with the diffractogram for the bare glass substrate and the JCPDS standard for cubic ZrO_2.

We can therefore conclude that spray pyrolysis for all investigated temperatures, concentrations and thicknesses on borosilicate glass led to the formation of cubic ZrO_2 films with (111) texture. The film thickness (which depends on the precursor concentration and scan number) and is highest for the deposition temperature of 410°C.

In Figure 13 the transmission spectra of the cubic ZrO_2 films, sprayed at temperatures between 360°C and 430°C are shown. While for the bare borosilicate glass a high transmittance of ~90% is reached, the ZrO_2-layers caused a reduction of the transmittance to almost ~45% in the visible field for the sample deposited at 410°C. The transmission for the film deposited at 410°C is slightly reduced, compared to the deposition that took place at 430°C, which is linked to the increased film thickness of the deposit prepared at 410°C.

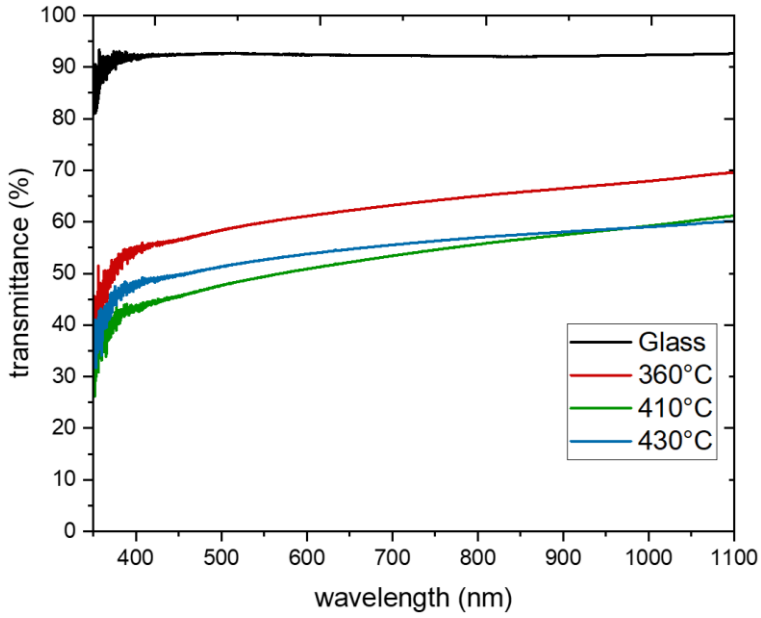

Figure 13: Optical transmission spectra of the cubic ZrO_2, sprayed at temperatures between 360°C and 430°C on borosilicate glass.

3.2. Properties of films deposited on FTO-coated glass substrates

For FTO, only two sets of experiments are presented: the variation in concentration and the temperature dependence on the film. The samples deposited for the "scan number variation" set are excluded, because of a deposition problem occurred during the spray process. The reason for this problem was probably linked to the incomplete cleaning of the FTO surface that adversely impacted the homogeneity of the ZrO_2 film growth.

Deposition of ZrO_2 on FTO from solutions with varying concentration

In a first set of experiments on the FTO substrates, the number of scanning repetitions was set to 200 and the temperature was held constant at 380°C. As in the previous experiments on glass, a higher precursor concentration leads to higher intensity peaks in the diffractogram. In Figure 14, the c-ZrO_2 (111) remains the dominant texture of the deposited ZrO_2 film for all concentrations. The peak gained in intensity with increasing of the deposition solution concentration. The ZrO_2 (200) peak appears as a shoulder on the right flank of the SnO_2 (101) peak. Likewise, the ZrO_2 (202) peak forms a shoulder at the left flank of the SnO_2 (211) peak.

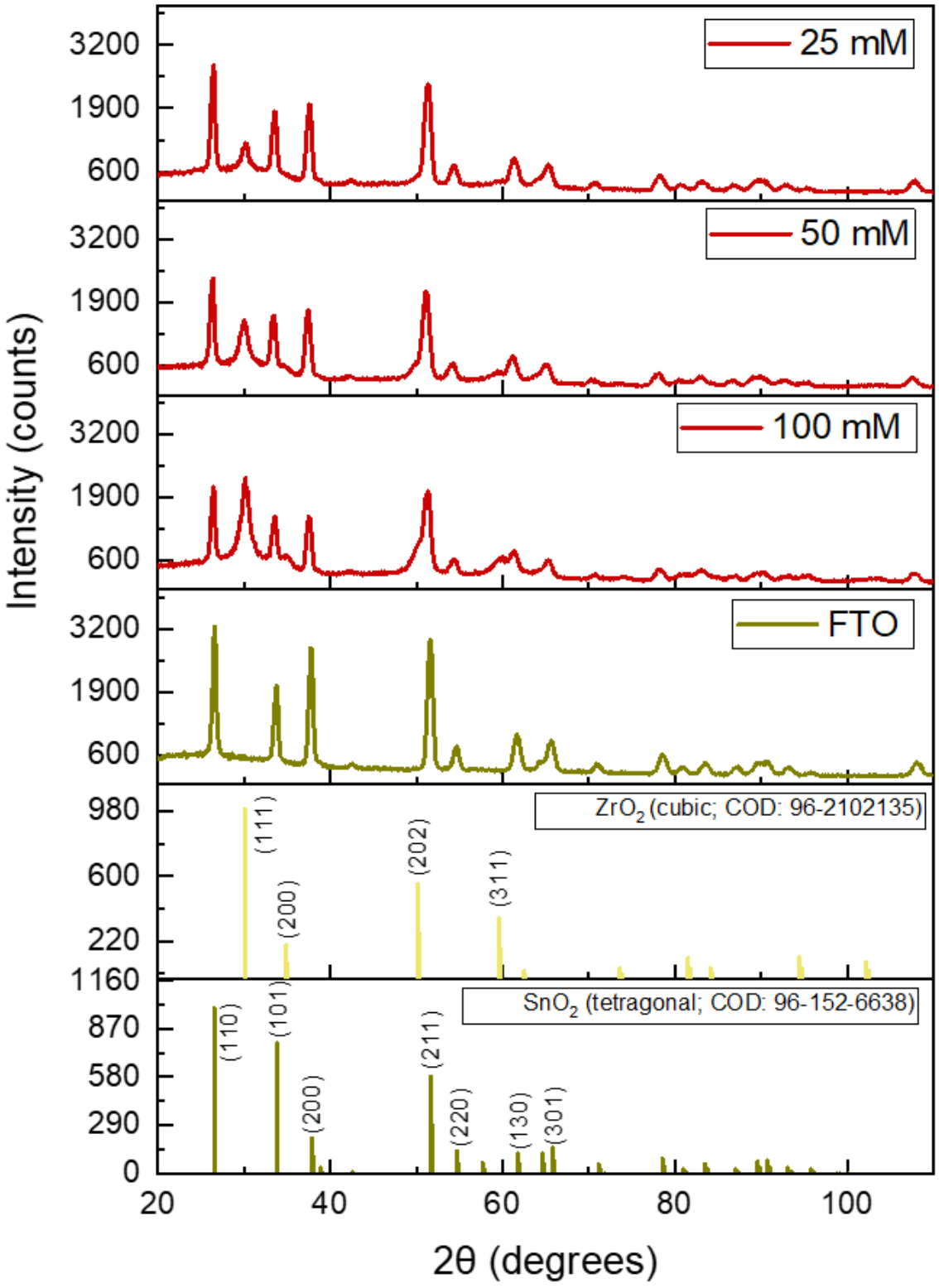

Figure 14: X-ray diffraction patterns of cubic ZrO_2 films, sprayed onto a substrate with a T=380°C at 200 scans, with varying concentrations of 25, 50 and 100 mM, on FTO-coated glass. Also shown is the glass/FTO substrate diffractogram and the JCPDS standards for the cubic ZrO_2 and tetragonal SnO_2.

The optical transmission spectra of as-deposited ZrO_2 films of various concentrations are shown in Figure 15. While the FTO substrate exhibits high optical transparency of up to 80 % in the visible to NIR region, a decrease in transmission is observed when films are deposited on FTO. For all three solution concentrations the disappearance of the FTO fringes is visible and can mainly be linked to the increase in thickness of the deposited layers.

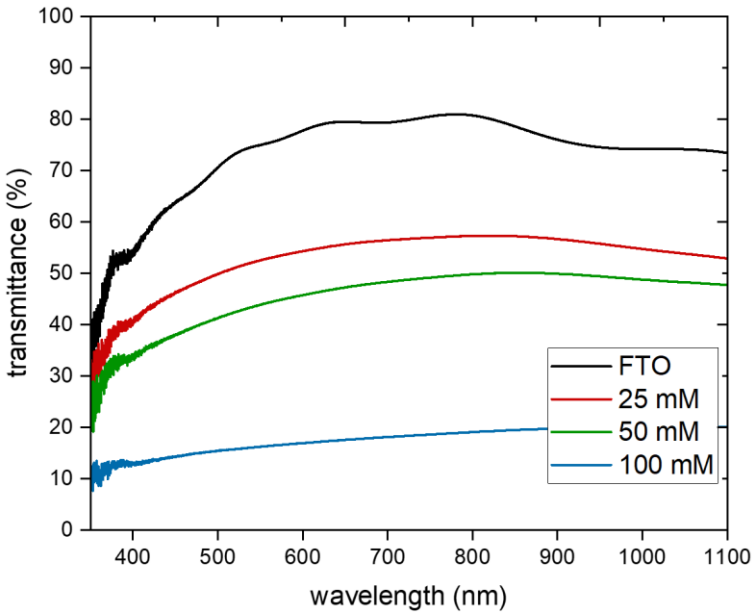

Figure 15: Optical transmission spectra of the cubic ZrO_2 films, sprayed at T=380°C and 200 scanning repetitions with varying solution concentration of 25, 50 and 100 mM on FTO-coated glass.

To evaluate the morphology of the deposited films, SEM micrographs at different magnifications were obtained for all tested solution concentrations. In all three concentration experiments, cross-sectional images were taken and are presented below.

The SEM micrographs of the sample deposited from the **25 mM** solution are presented figure 16, together with those of the reference FTO substrate. The surface images of the deposits show a high density of overlapping rings, suggesting the impact of droplets onto the substrate and the subsequent formation of the film from these droplets, as the solvent evaporated (Fig. 16a, 16b and 16d). In this sense, we can conclude that the deposition, at least in its major part, did not take place from the vapour phase, as would have been the ideal case. Between the ZrO_2 film deposits and the FTO substrate, a distinctive contrast is visible. Some areas of the FTO substrate remain uncovered, as the characteristic grain structure of the FTO is clearly observed (Fig. 16c). The cross-section images agree with the inhomogeneous deposition. However, the

formation of a ZrO_2 film on top of the FTO can be clearly observed (Fig. 16f - h). The approximate ZrO_2 film thickness is ~300 nm.

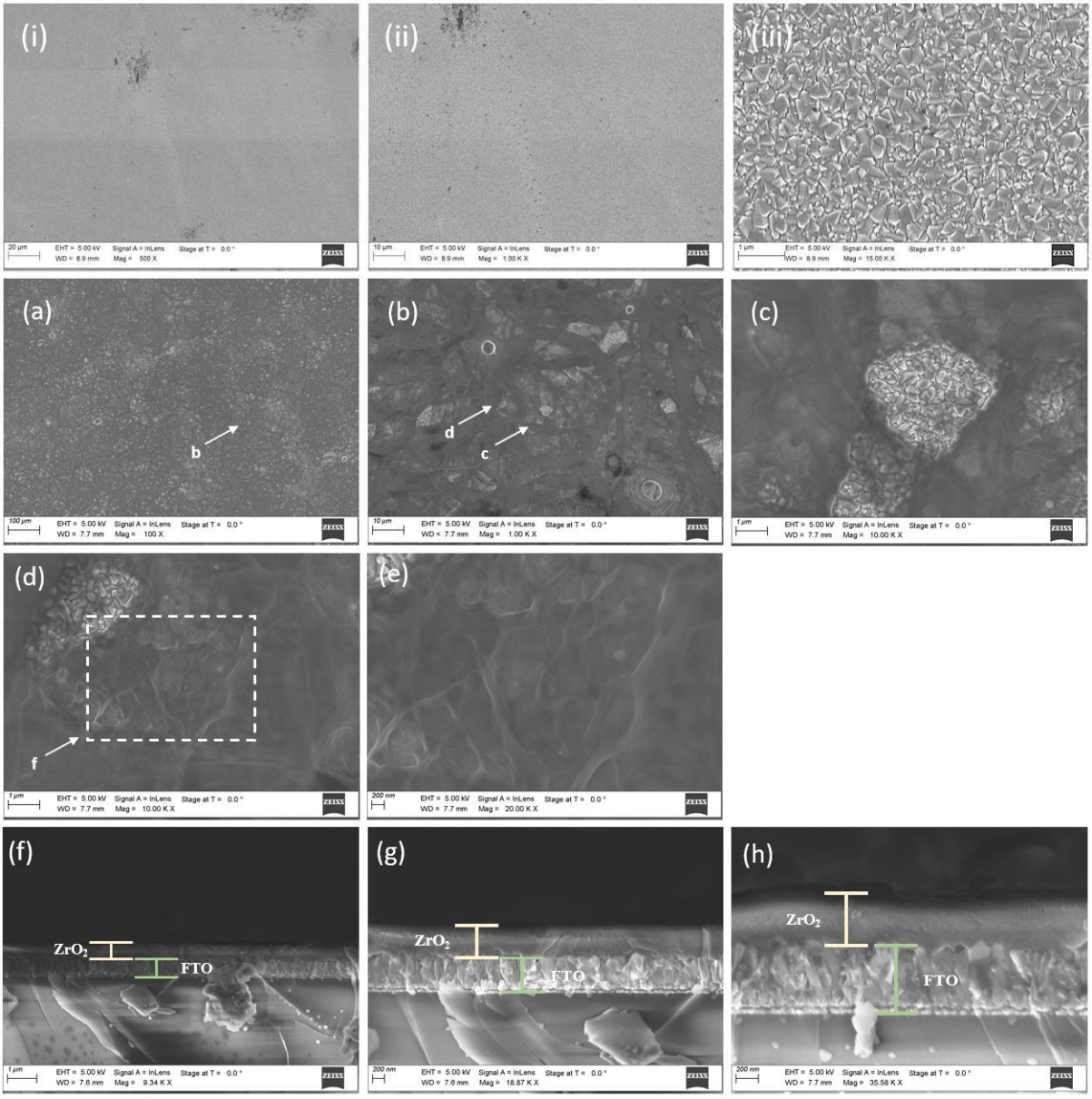

Figure 16: i)-iii) SEM micrographs of the glass/FTO substrate. a)-e) Plane-view and f)-h) cross-section SEM micrographs of the FTO/ZrO_2 layer deposited from the 25 mM concentration solution.

An increase of the concentration to 50 mM resulted in increased substrate coverage and larger film thickness (see cross-section images in Fig. 17e and 17f). The thickness is extracted ~800 - 1000 nm. Here, the rings stemming from the droplet impact are not as visible as in the previous example, but the deposition remained inhomogeneous (Fig. 17b and 17c) and areas of the FTO substrate remained uncovered, as seen in Fig. 17a and 17d.

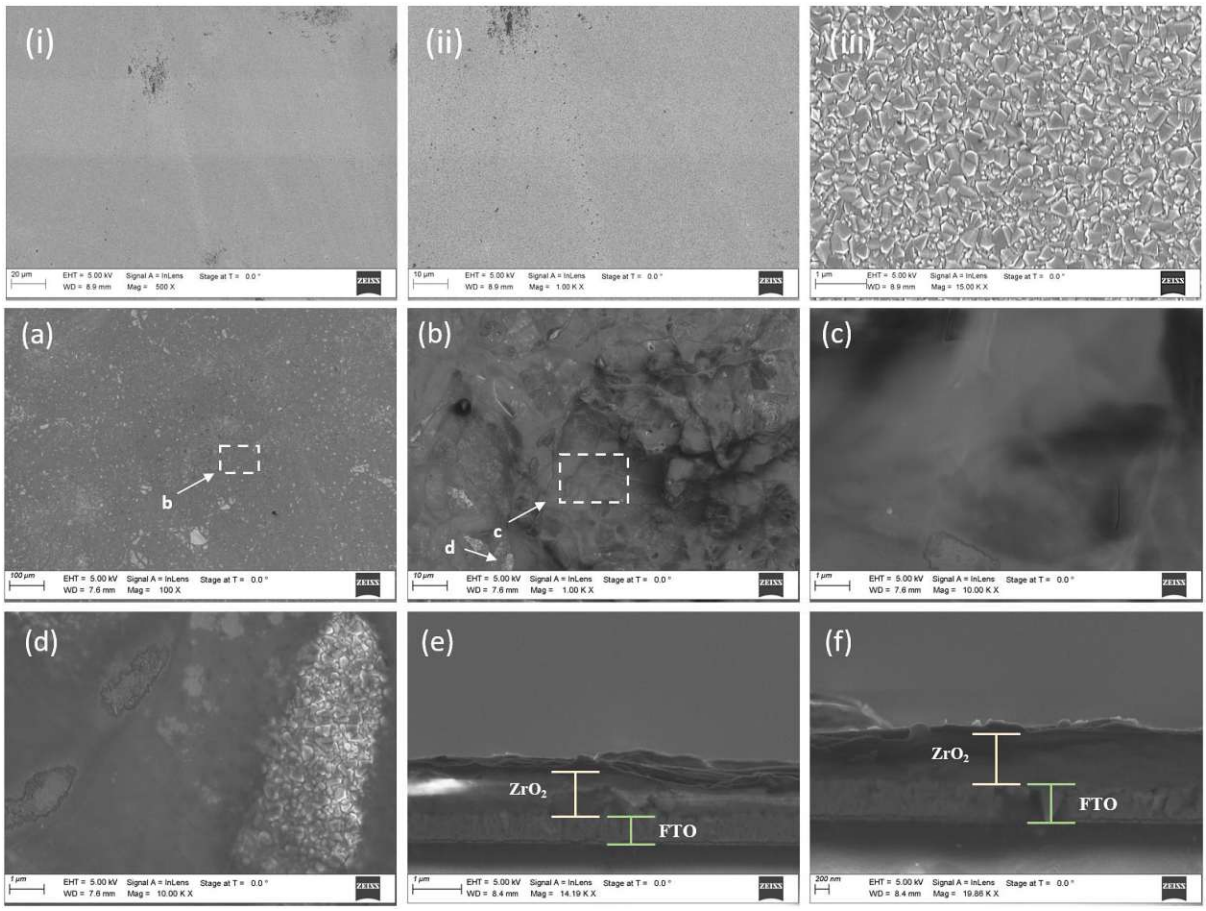

Figure 17: i)-iii) SEM micrographs of the glass/FTO substrate. a)-d) Plane-view and e)-f) cross-section SEM micrographs of the FTO/ZrO_2 film deposited from the 50 mM solution

The highest tested concentration was 100 mM. SEM images of the deposited material and the reference FTO are presented in Fig. 18. The observations made for the previous cases regarding film growth still hold in this case and again areas of the substrate remained uncovered. However, the film thickness increased further to >1.5 µm (see cross-section images in Fig. 18d to 18f), giving rise to the more pronounced XRD peaks seen in the previous section.

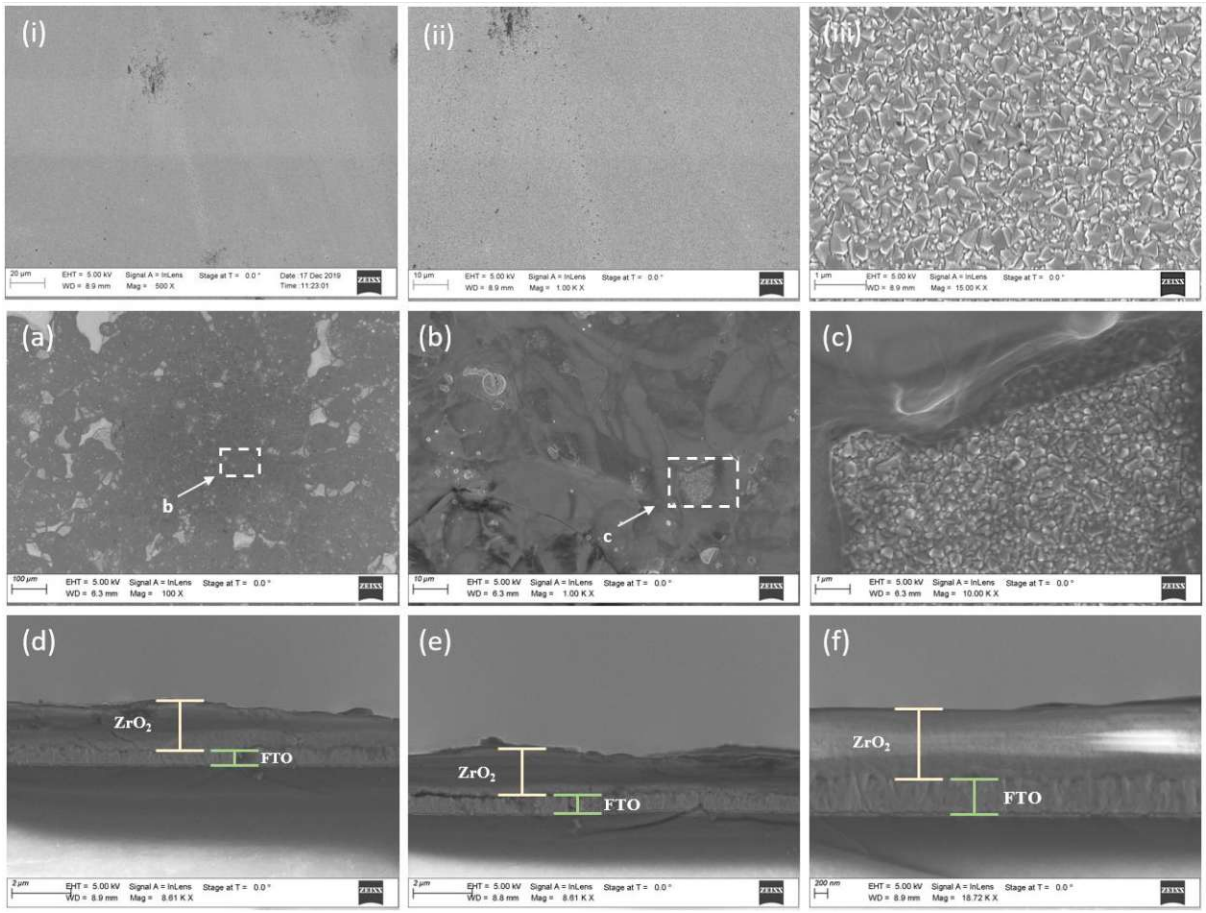

Figure 18: i)-iii) SEM micrographs of the glass/FTO substrate. a)-c) Plane-view and d)-f) cross-section SEM micrographs of FTO/ZrO_2 film deposited from the 100 mM solution

Depositions on FTO with varying temperature

To investigate the effect of the substrate temperature on the ZrO_2 deposition, the scanning repetitions were set to 250 and the concentration of the solutions was held constant at 100 mM. For FTO-coated glass, temperatures of 360, 380 and 410°C were investigated. The X-ray diffractograms of the ZrO_2 films deposited on FTO-coated substrates at different temperatures are shown in Figure 19. Also shown is the diffractogram of the FTO-coated glass (without deposited ZrO_2) and the standards for cubic ZrO_2 and tetragonal SnO_2.

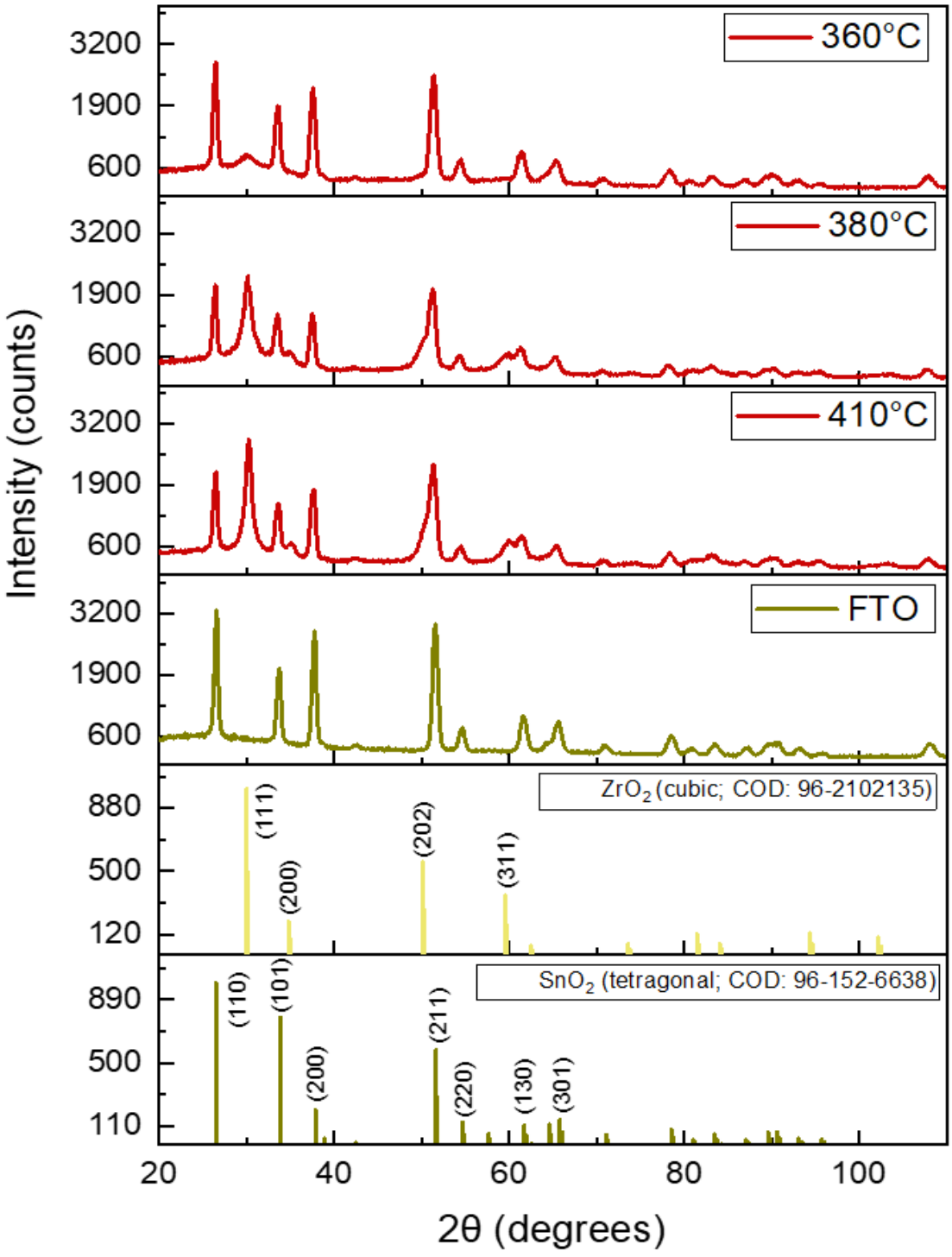

Figure 19: X-ray diffraction patterns of the cubic ZrO_2 films, sprayed at temperatures between 360°C and 410°C on FTO-coated glass, along with the diffractogram for the glass/FTO substrate and the JCPDS standard for cubic ZrO_2 and tetragonal SnO_2.

The peaks of the deposited ZrO_2 match well with the cubic ZrO_2 (COD-ID: 96-210-2135). The film deposited at the lowest temperature of 360°C has the lowest intensity peaks, with the most prominent peak being the (111). The (202) and (311) reflections have a lower intensity and are better visible when the substrate temperature was 380°C and 410°C. The dominant texture of the deposited ZrO_2 films remains (111). Apart from the previously mentioned peaks, now the

(200) peak is also clearly visible. As previously described in the experiment where the concentrations were varied, here also the ZrO_2 (200) and (202) peaks appear as shoulders on the flanks of the SnO_2(101) and (211) peaks.

We can therefore conclude that the spray pyrolysis for all investigated temperatures led to the formation of cubic ZrO_2 films with (111) texture. The film texture increased as the deposition temperature increased.

To evaluate the morphology of the deposited films, SEM micrographs at different magnifications were obtained for films produced at all tested temperatures. To facilitate comparison, reference micrographs of bare FTO in the corresponding magnifications were also taken and are presented in the figures, labelled with roman numerals.

The SEM micrographs of the ZrO_2 deposited at **360, 380 and 410°C** are shown in Fig. 20, 21 and 22, respectively. For all temperatures, the SEM images indicate that the film formation is consistent with droplet impact and subsequent growth from the liquid phase. This is supported by the overlapping ring formations in the plain view images and the incomplete coverage of the FTO substrate.

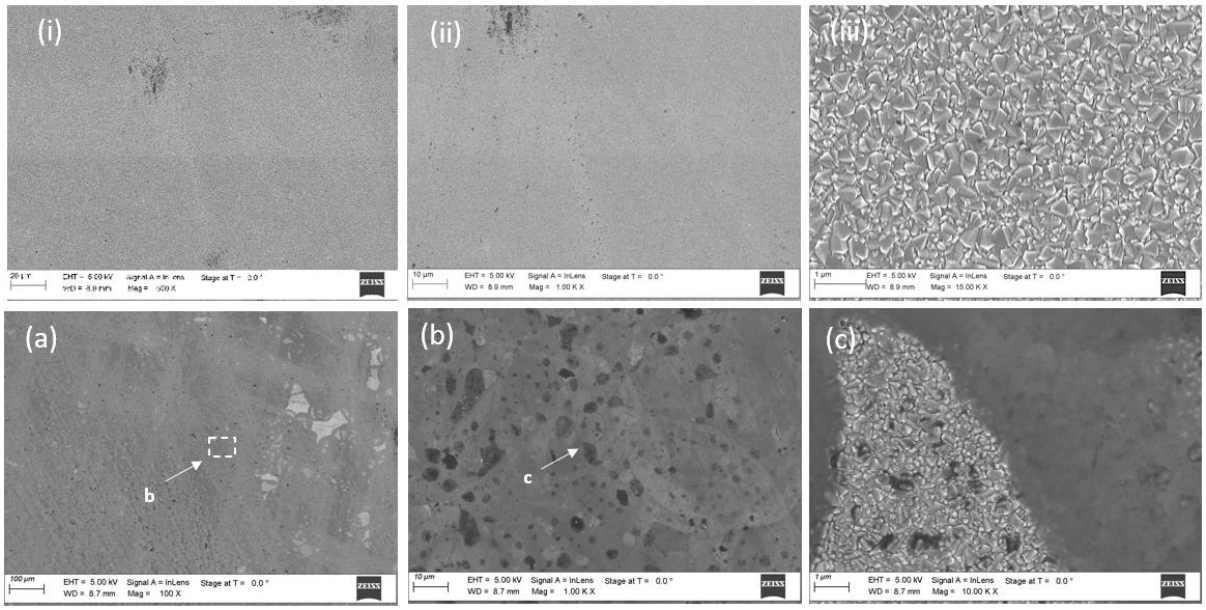

Figure 20: i)-iii) SEM micrographs of the glass/FTO substrate. a)-c) Plane-view SEM micrographs of FTO/ZrO_2 film deposited at 360°C.

At low magnification (Fig. 21a) the sample surface of the deposition at **380°C** features circular-shaped residuals that can be linked to incomplete evaporation of the solvent and the impact of droplets on the substrate. In Fig. 21d bulky and thin deposition is visible. Enlarging into the region of the "spherical shaped edge" a difference in brightness is visible, which implies the

occurrence of thin deposit (spot 21f1) and bare FTO (21f2). The cross-section SEM images also show locations where bulk deposits can be seen (Fig. 21g) and other locations where the deposit is very thin (Figure 21h and 21i). This agrees with the scenario of droplet impact on the substrate, resulting in spatially inhomogeneous deposits.

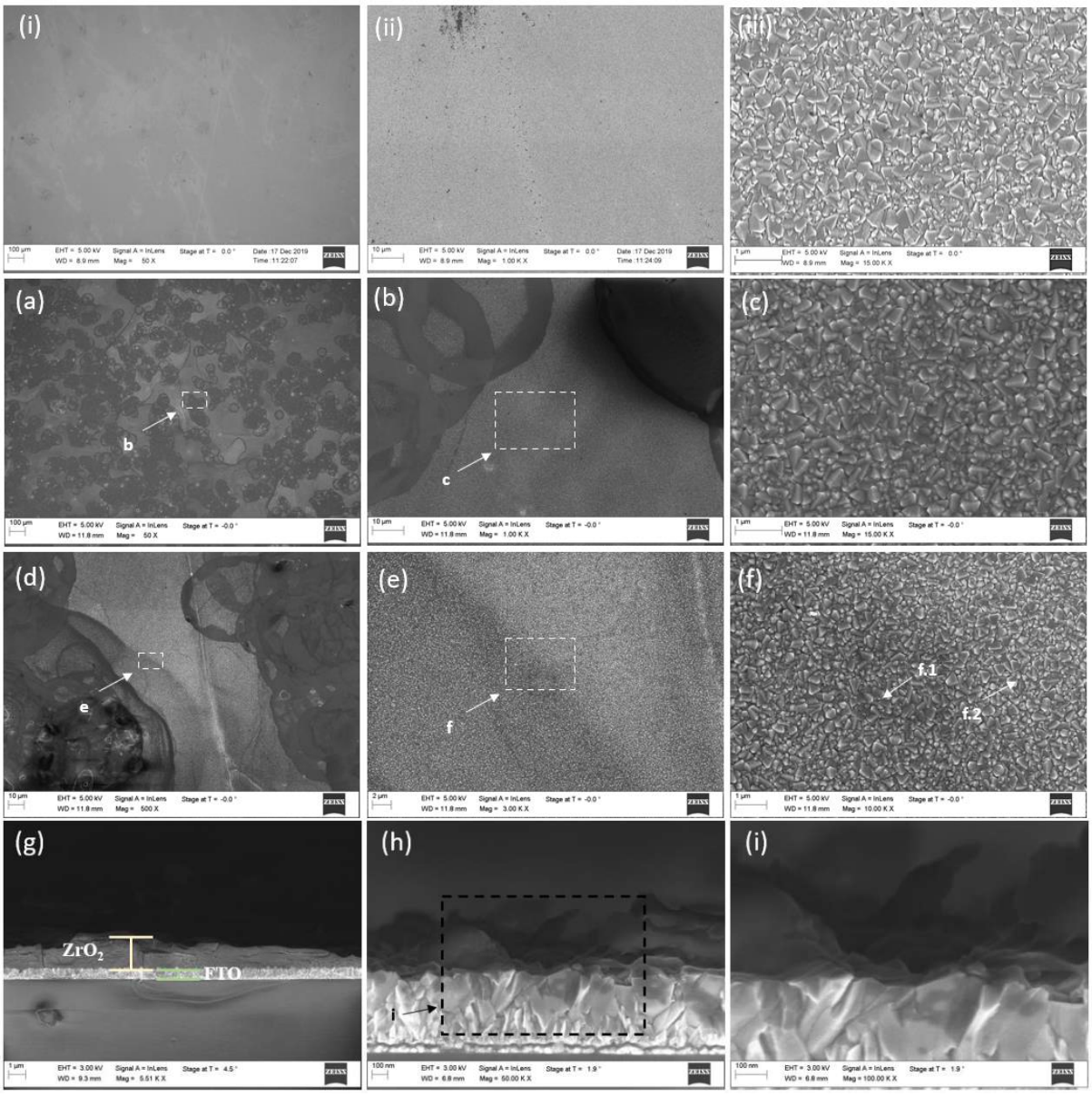

Figure 21: i)-iii) SEM micrographs of the glass/FTO substrate. a)-f) Plane-view and g)-i) cross-section SEM micrographs of FTO/ZrO_2 film deposited at 380°C.

The surface of the film produced on substrates with T=**410°C** shows again inhomogeneous deposition. In some locations of the sample (Fig. 22i), a grain structure that distinguishes itself from the one of the FTO substrate or from the surrounding deposit (Fig. 22f), can be observed that is suggestive of growth from the vapor phase.

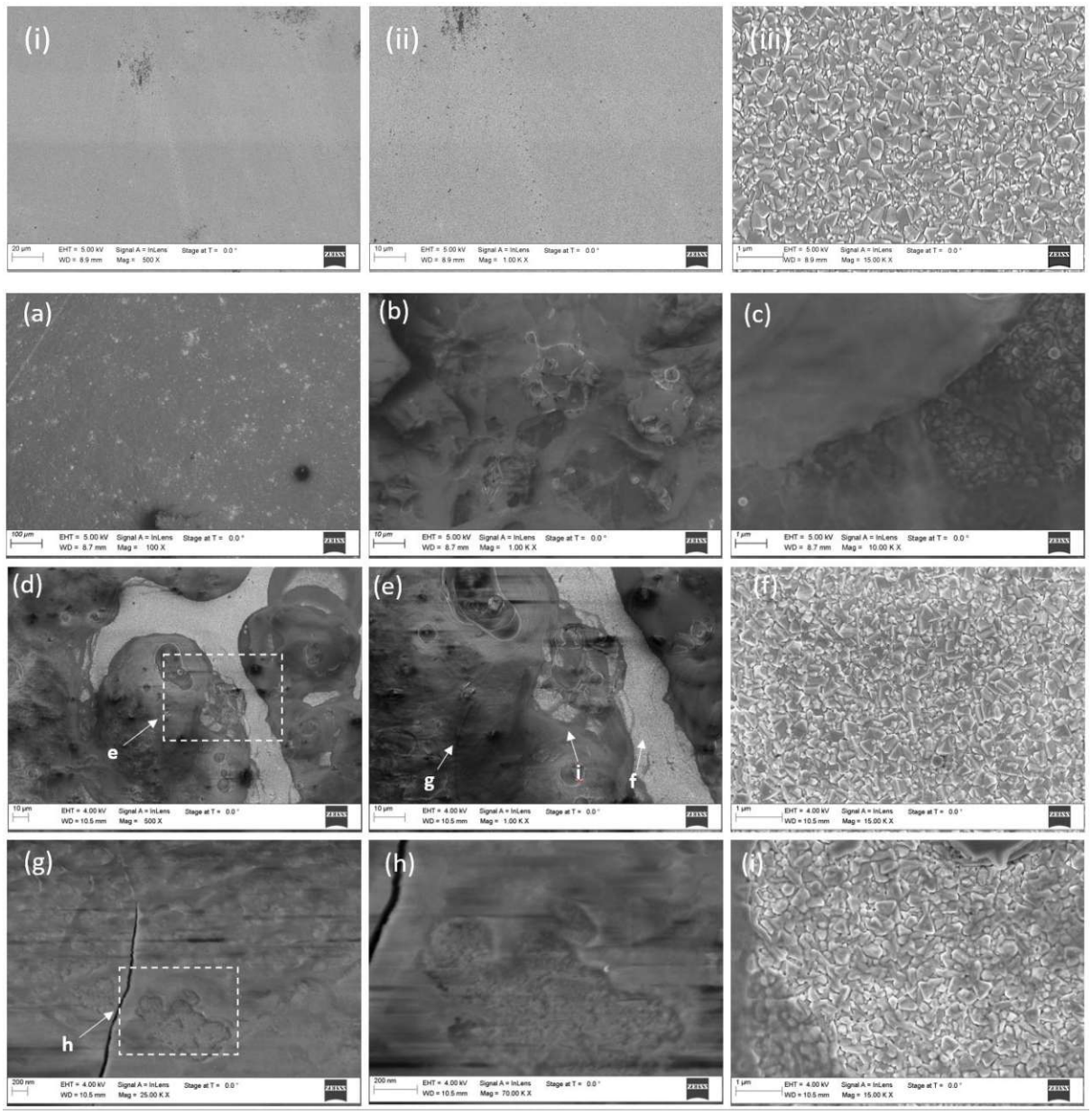

Figure 22: i)-iii) SEM micrographs of the glass/FTO substrate. a)-i) Plane-view SEM micrographs of FTO/ZrO_2 film deposited ZrO_2 at 410°C.

No optical transmission spectra for this experiment set are presented, due to cracks in the films that were visible to the naked eye and appeared on the sample surface after the deposition process.

3.3. Properties of the film deposited on ITO-coated glass substrates

Deposition with varying solution concentration on ITO

The positions of the ZrO_2 and FTO X-ray reflection peaks are located in distinctive angles, which makes their separation straight-forward in the diffractograms. This is not the case for the peaks of cubic ZrO_2 and ITO, for which the peak positions are very similar. Though, to a certain degree, we can draw conclusions about the development of texture in the ZrO_2 layer by comparing the peak intensities of the bare ITO substrate as opposed to the ones coated with ZrO_2. In Figure 23 we can see the diffractograms of the ZrO_2 films on ITO-coated glass substrates for solution concentrations of 25, 50 and 100 mM, together with the diffractogram of bare ITO and the standards for cubic ZrO_2 and cubic In_2O_3.

The peaks corresponding to the ZrO_2 (111) and In_2O_3 (222) reflections are the most prominent in all cases. All peaks gained in intensity with increasing precursor concentration, suggesting that this is caused by the increase of the thickness of the deposited ZrO_2 film, in accordance to what was observed in the case of the bare glass and FTO substrates.

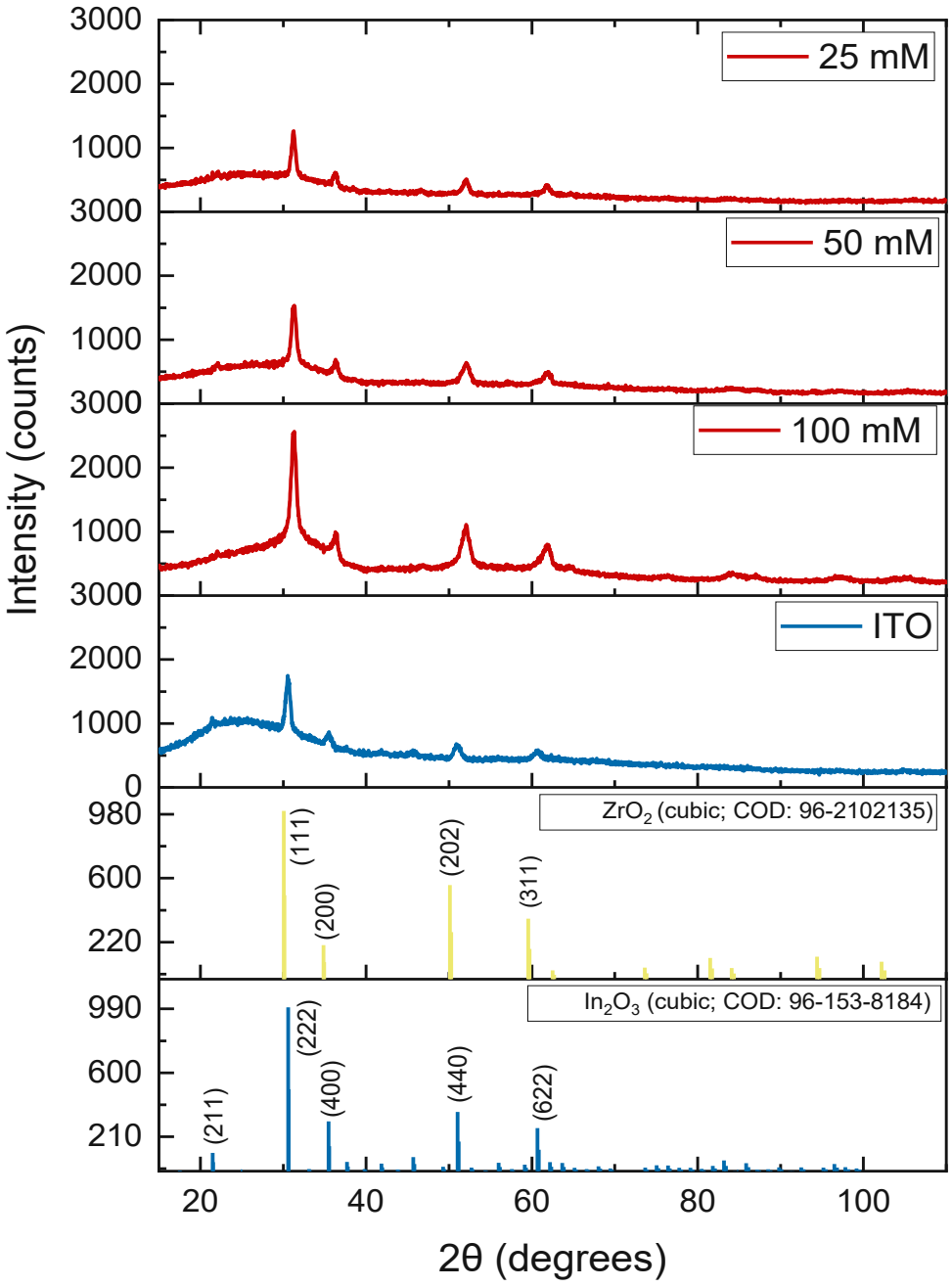

Figure 23: X-ray diffraction patterns of the cubic ZrO_2 films, sprayed onto a substrate with a T=380°C at 200 scans, with varying concentrations of 25, 50 and 100 mM, on ITO-coated glass. Also shown is the glass/ITO substrate diffractogram and the JCPDS standards for the cubic ZrO_2 and cubic In_2O_3.

The optical transmission spectra measured for ITO substrates coated with ZrO_2 from solutions with varying concentration are presented in Figure 24. As with the previous examples, an increase of concentration leads to a reduction of the transmittance, which is linked to the increased film thickness. For the highest concentration of 0.1 M a reduction of the transmittance of down to ~10% in the visible region was observed. This can be linked to the presence of precipitates on the surface.

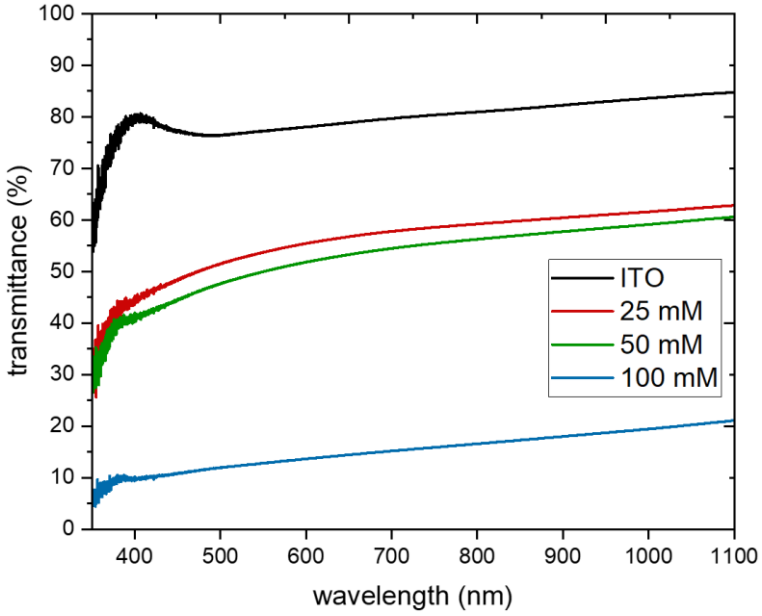

Figure 24: Optical transmission spectra of the cubic ZrO_2 films, sprayed at T=380°C and 200 scanning repetitions with varying solution concentration of 25, 50 and 100 mM on ITO-coated glass.

To evaluate the morphology of the deposited films, plain view and cross-section SEM micrographs were obtained. These are shown in Fig. 25, 26, and 27 for ZrO_2-coated substrates deposited with precursor solution concentrations of **25, 50 and 100 mM**, respectively. The following conclusions can be drawn from the SEM investigation:

Firstly, the ZrO_2 layer thickness increases with increasing precursor solution concentration. This is especially obvious if we compare the cross-section images of the ZrO_2 film produced using the 100 mM with those of lower concentrations (Fig. 27d and 27e, Fig. 25g to 25i). For the films made from the 25 mM solution the thickness is ~300 nm, from the 50 mM solution ~700 nm and from 100 mM ~1.5 µm.

Second, the growth mode on ITO seems to be more of a mixed nature. There are still overlapping ring formations (Fig. 26b) suggesting droplet impact on the substrate, but there is also more distinctive grain formation (Fig. 26f) but the ZrO_2 deposit is more homogeneous, as compared to that on FTO, which may point out to an increased contribution from a CVD-type of growth. Visually the samples are also more homogeneous than the ones on FTO, resembling the ZrO_2 on plain glass. Unfortunately, due to the insulating substrate and the induced charging, we could not evaluate by SEM the samples on plain glass.

One of the reasons why on ITO the deposition seems to be more homogeneous can be that the glass/ITO substrate is only 1 mm thick, compared to 2.2 mm for the glass/FTO. The differences

in the thermal capacity can lead to differences in the effective temperature of the substrate, which in turns will influence the growth mode.

The deposits created with the lowest concentration of **25 mM** are visible in Fig. 25. The ZrO_2 deposits in 25a 25b and 25c can mainly be linked to incomplete evaporation of the solvent and the impact of droplets on the substrate. At some locations (as shown in Fig. 25e) grains are visible that indicate the deposition from the vapor phase while other locations (Fig. 25f) indicate a deposition originating from the liquid phase.

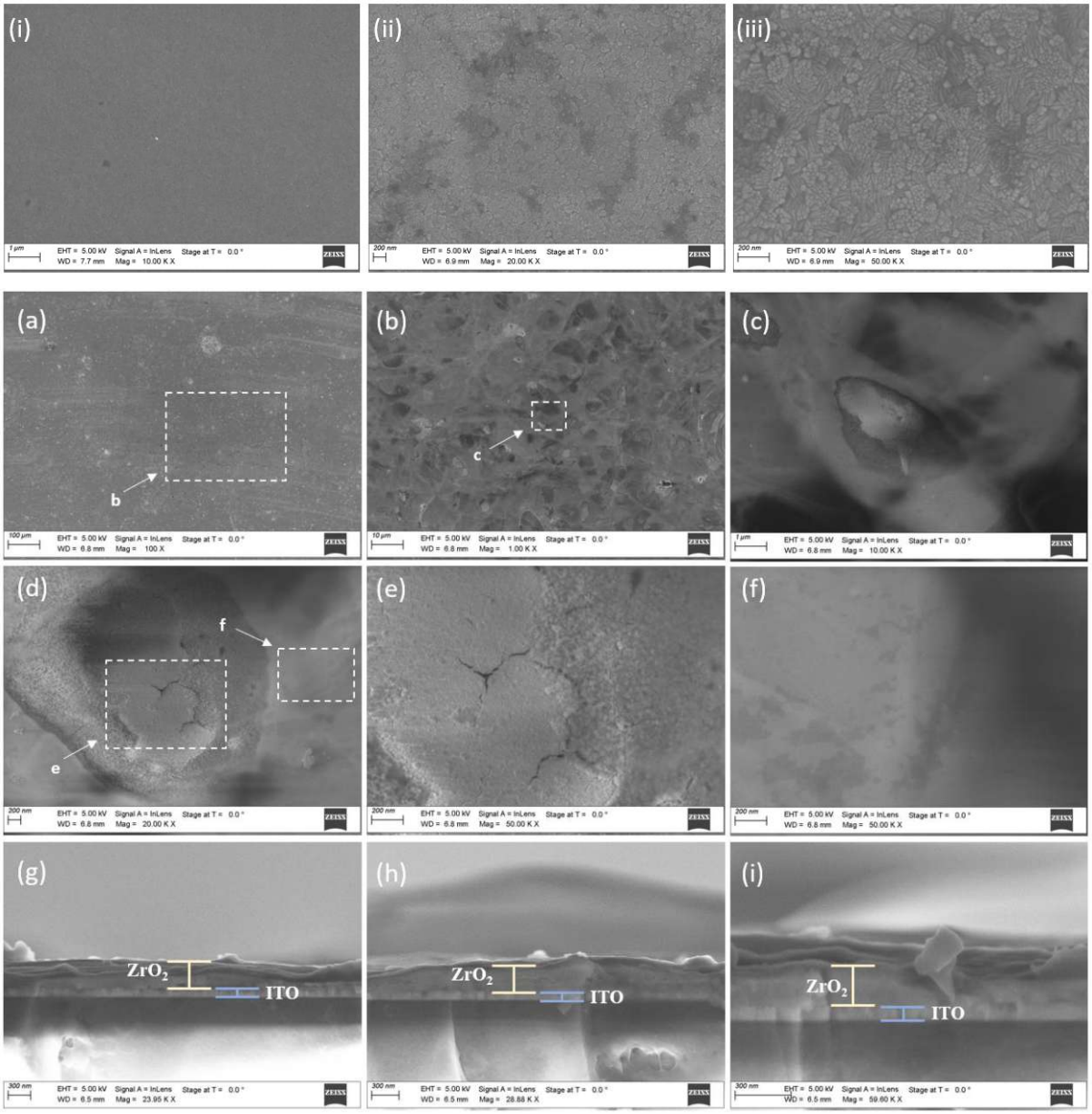

Figure 25: i)-iii) SEM micrographs of the glass/ITO substrate. a)-f) Plane-view and g)-i) cross-section SEM micrographs of the ITO/ZrO_2 layer deposited from the 25 mM concentration solution.

When using a precursor concentration of **50 mM** similar data was observed as with the previous example. Magnifying into different sample locations (as shown in 26d, 26e and 26f) grain growth is visible underneath the bulky material. The cross-sections also show bulk deposits.

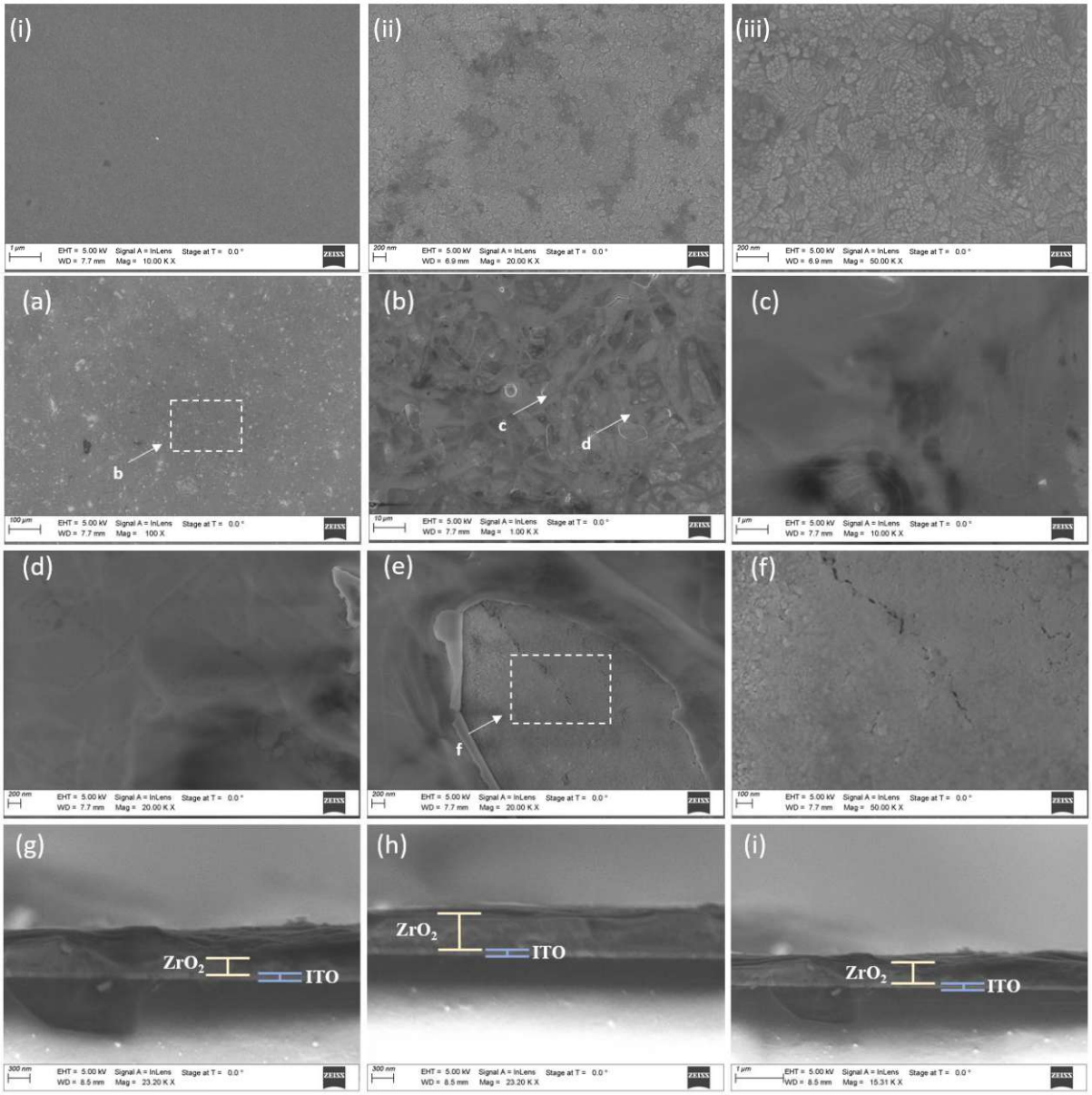

Figure 26: i)-iii) SEM micrographs of the glass/ITO substrate. a)-f) Plane-view and g)-i) cross-section SEM micrographs of the ITO/ZrO_2 layer deposited from the 50 mM concentration solution.

The plane view and cross-sectional micrographs of the sample created with a precursor concentration of **100 mM** are presented in Fig. 27. What under low magnifications seems to be uncovered, light spots (as visible in Fig. 27a), appear to be bulky and inhomogeneous material deposits at higher magnifications (Fig. 27b and 27c).

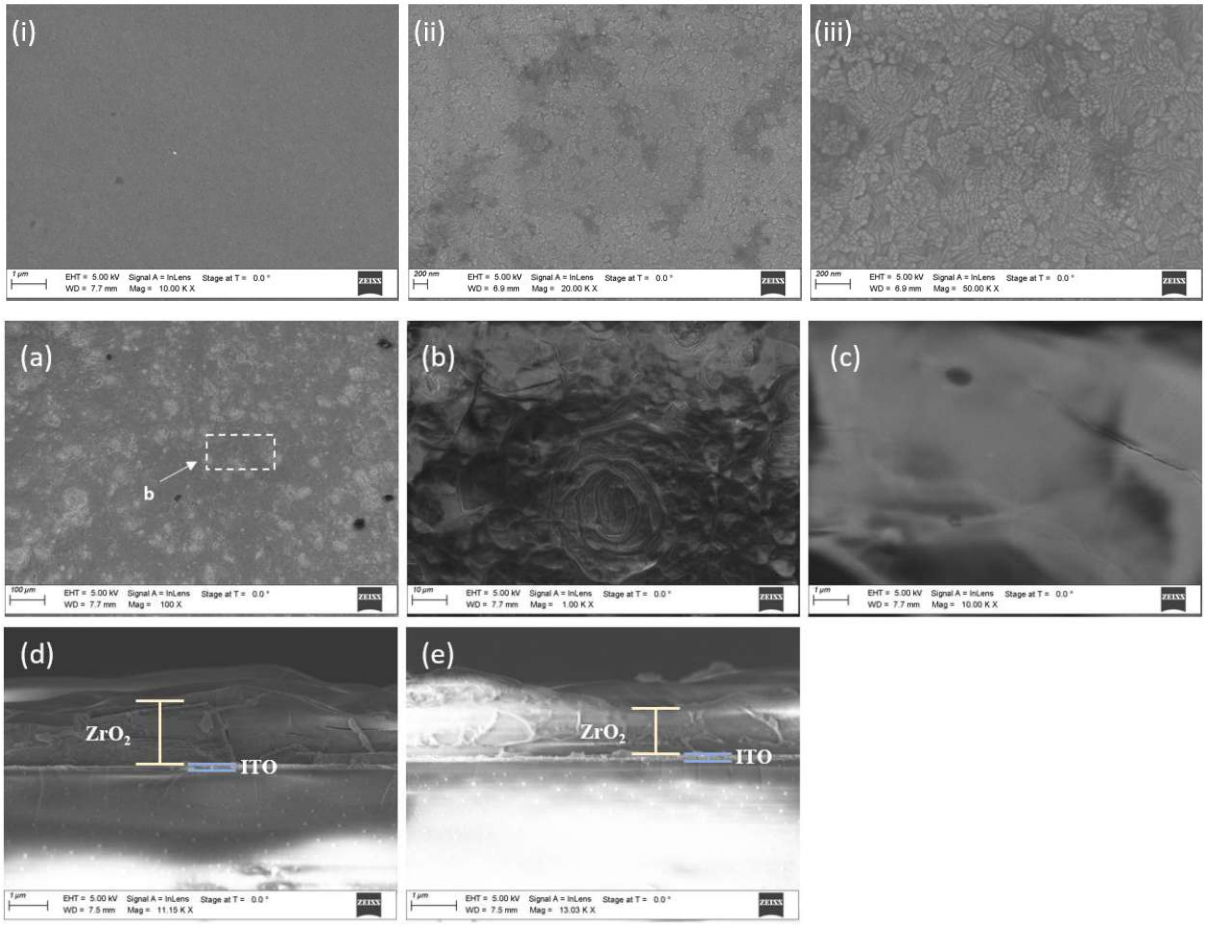

Figure 27: i)-iii) SEM micrographs of the glass/ITO substrate. a)-c) Plane-view and d)-e) cross-section SEM micrographs of the ITO/ZrO_2 layer deposited from the 100 mM concentration solution.

Deposition with varying scan number on ITO

In a second set of experiments, the deposition temperature was held constant at 410°C and the scan number was varied from 100 to 250. The target was to probe the development of texture the ZrO_2 thickness increased. Indeed, we observe a tendency of increasing reflection peaks amplitude with increasing number of scans, consistent with what has been observed in the case of the deposition on glass and glass/FTO substrates.

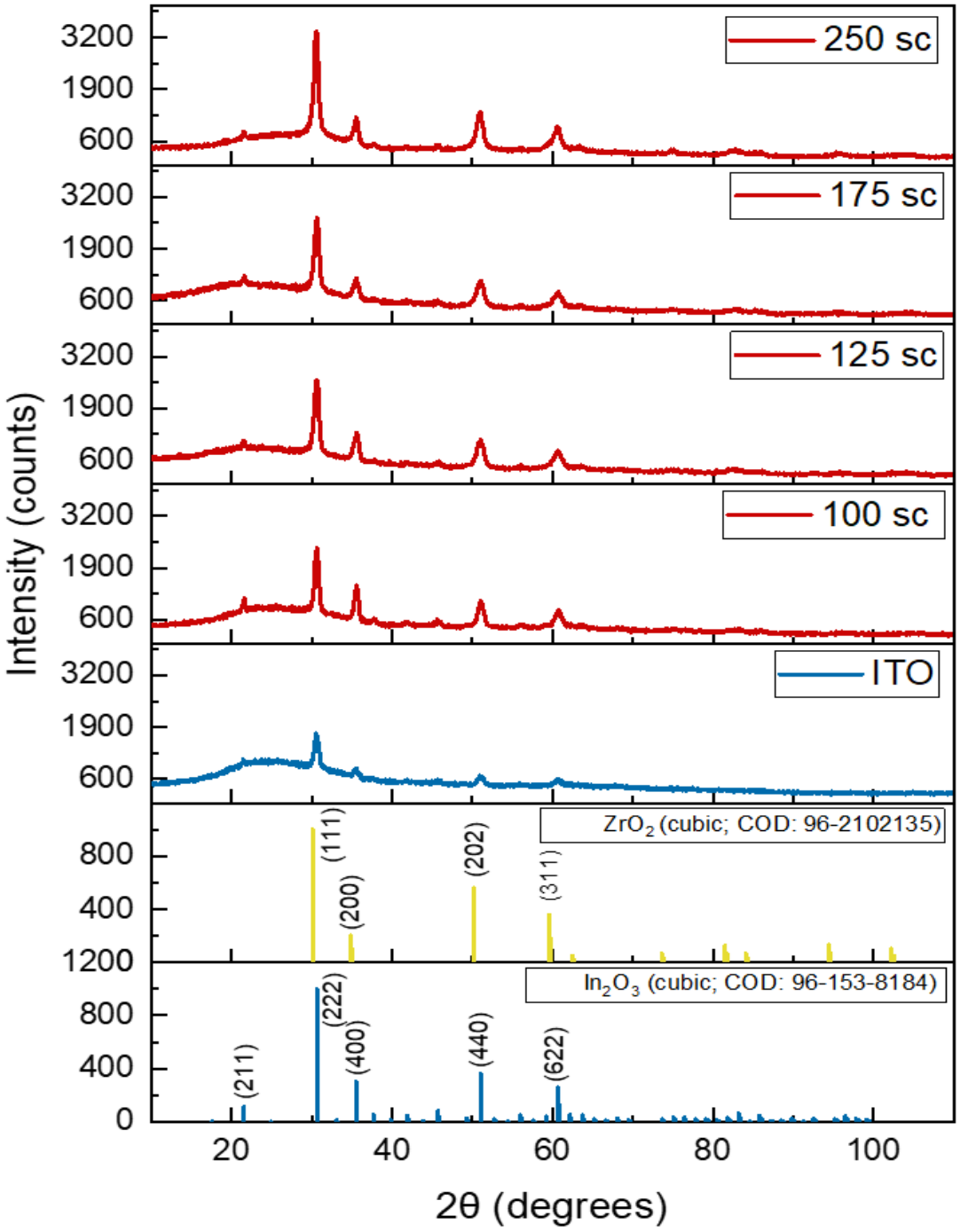

Figure 28: X-ray diffraction patterns of the cubic ZrO_2 films, sprayed at T=410°C and c=100 mM with scanning numbers varying between 250 and 100 on ITO-coated glass. Also shown is the glass/ITO substrate diffractogram and the JCPDS standards for the cubic ZrO_2 and cubic In_2O_3.

In Figure 29, the transmission spectra of the bare ITO and the deposited zirconium oxide layers show again the effect of increasing coverage of the sample, with increasing scan number.

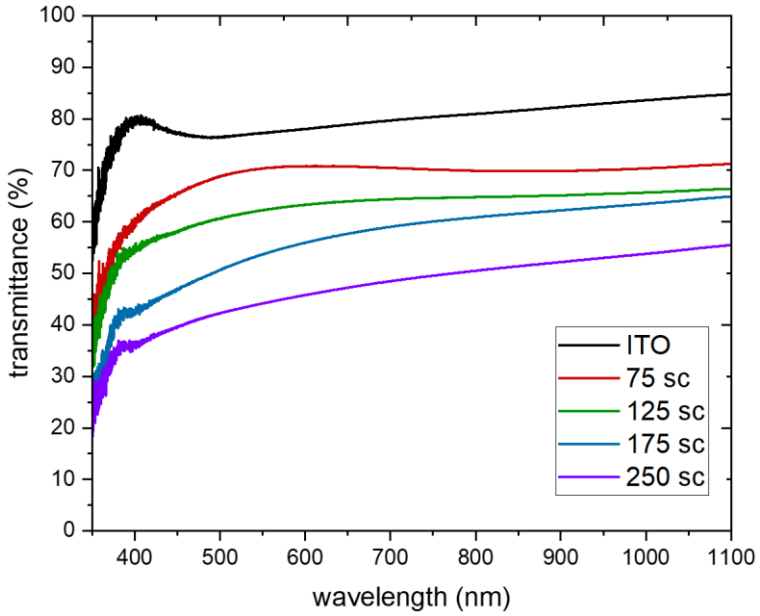

Figure 29: Optical transmission spectra of the cubic ZrO_2 films sprayed at T=410°C and c=100 mM on borosilicate glass with scanning number varying between 250 and 100 scans (sc).

Depositions with varying temperature on ITO

On the ITO substrate, substrate temperatures between 360°C and 430°C have been tested. With a constant concentration of 100 mM and 250 scanning repetitions, the X-ray diffractograms of the samples are shown in Figure 30. Once more, in all deposited films the (111) orientation dominates. The peak amplitude is highest when using 410°C as the substrate temperature, suggesting highest thickness/better crystallization for the film at this temperature.

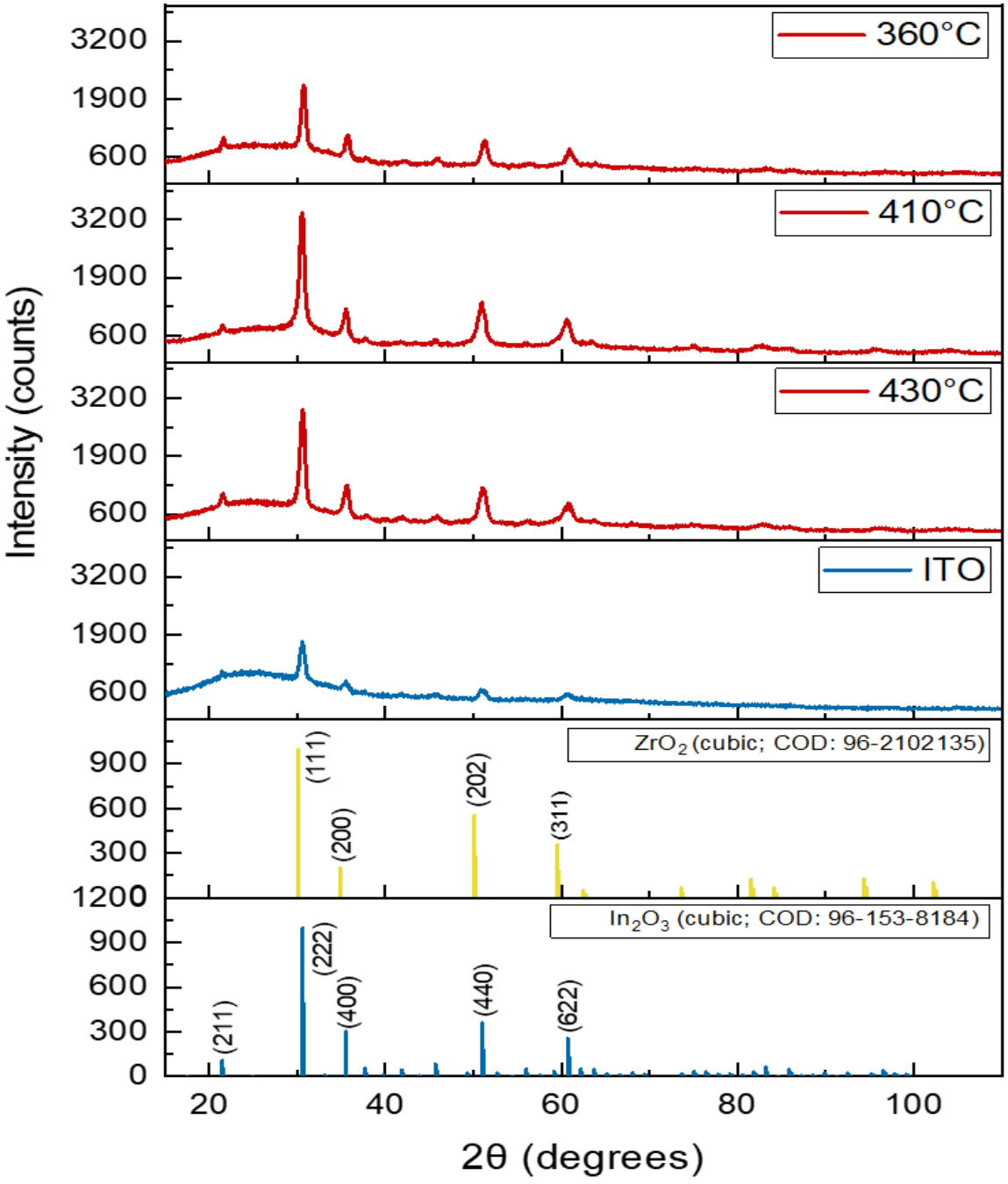

Figure 30: X-ray diffraction patterns of the cubic ZrO_2 films, sprayed at temperatures between 360°C and 430°C on ITO-coated glass, with their corresponding JCPDS standards for cubic ZrO_2 and cubic In_2O_3.

In Figure 31 the transmission spectra of the cubic ZrO_2 films, sprayed onto substrates with temperatures between 360°C and 430°C is shown. While for the bare ITO a high transmittance is reached, the ZrO_2-layers show a reduction of the transmittance to almost ~35% in the visible field. Like in section 3.1, where the borosilicate substrate was discussed, the increased film thickness of ZrO_2 films produced on substrates with 410°C sample is responsible for the reduction of the transmittance, compared to 360°C and 430°C.

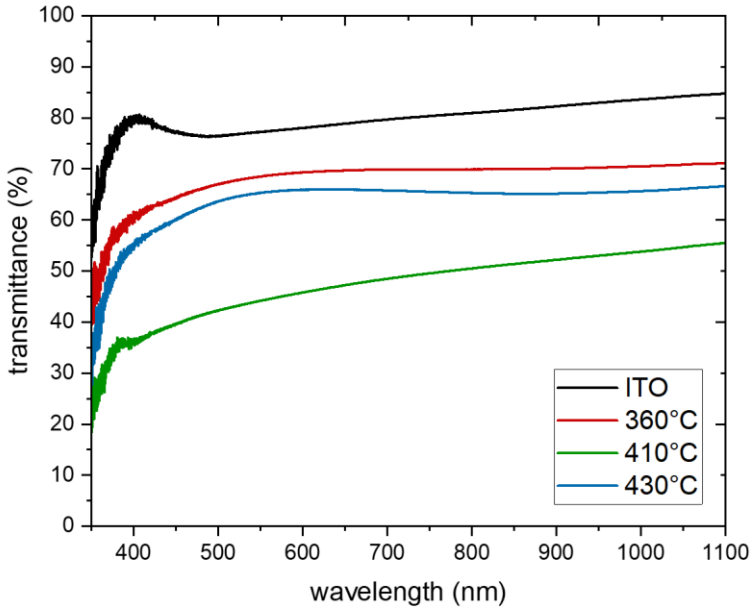

Figure 31: Optical transmission spectra of the cubic ZrO_2, sprayed at temperatures between 360°C and 430°C on ITO-coated glass.

The SEM images for the ZrO_2 films produced on substrates with temperature of **360, 410 and 430°C** are shown in Fig. 32, 33, and 34, respectively. The drawn conclusions are aligned with the ones of the previous experimental set: a mixed growth from the liquid and from the vapour seems to prevail for all temperatures, even for the lowest of 360°C. Indeed, in certain locations we see darker contrast, which is, based on our interpretation, stemming from growth from the liquid phase (Fig. 32d). This is combined with regions with lighter contrast, corresponding to a well-formed grain structure (clearly different from the one of the underlying ITO substrates), compatible with CVD-type growth (Fig. 32f).

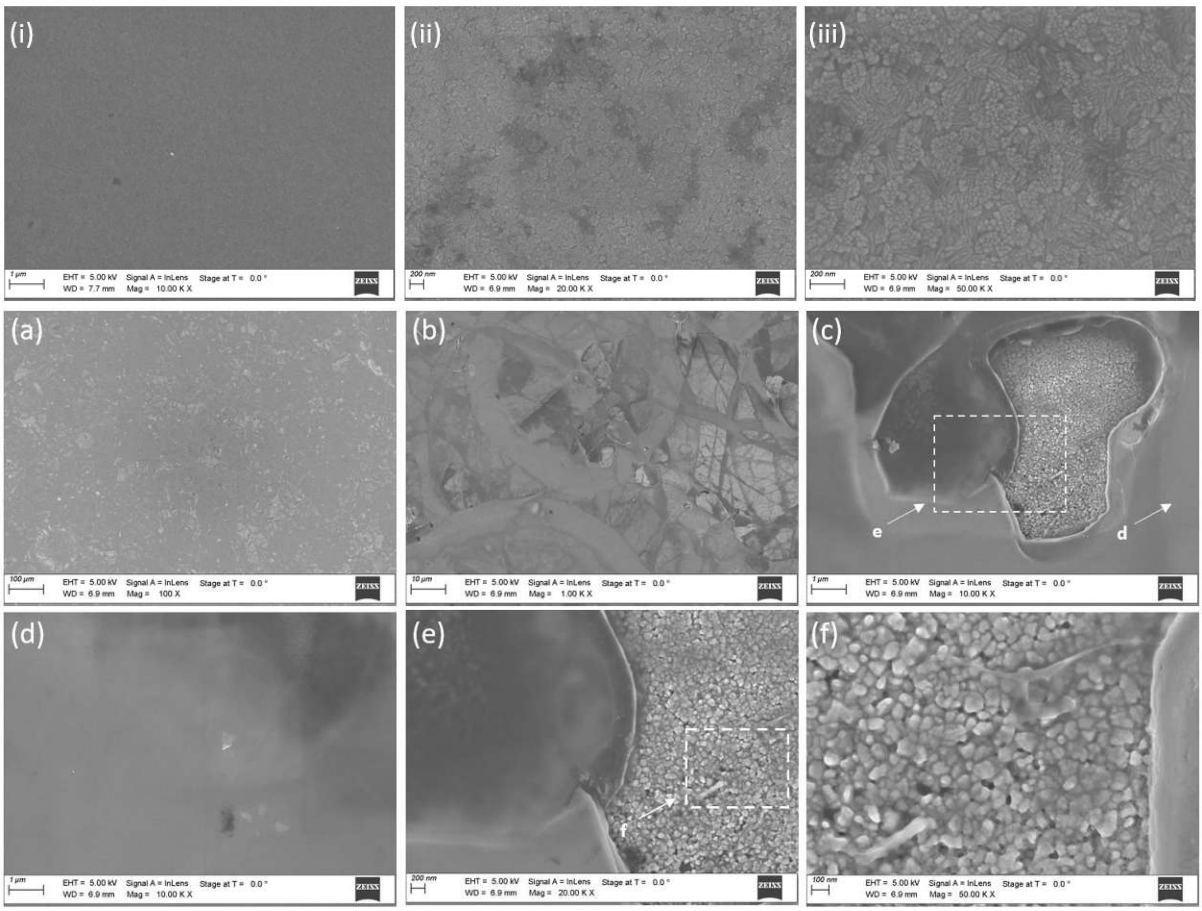

Figure 32: i)-iii) SEM micrographs of the glass/FTO substrate. a)-f) Plane-view SEM micrographs of FTO/ZrO_2 film deposited ZrO_2 at 360°C.

The plain view micrographs of a ZrO_2 film produced on ITO with T=410°C are mainly covered with darker regions and unlike in the previous examples, the amount of regions with light contrast is rather low. Cross-sectional micrographs were also obtained. The deposition shows a “rather thick” coverage of ITO. The deposition visible above ITO with a thickness of ~150 nm in 33g) and 33h) is the deposition of ZrO_2 with a film thickness of ~500 nm.

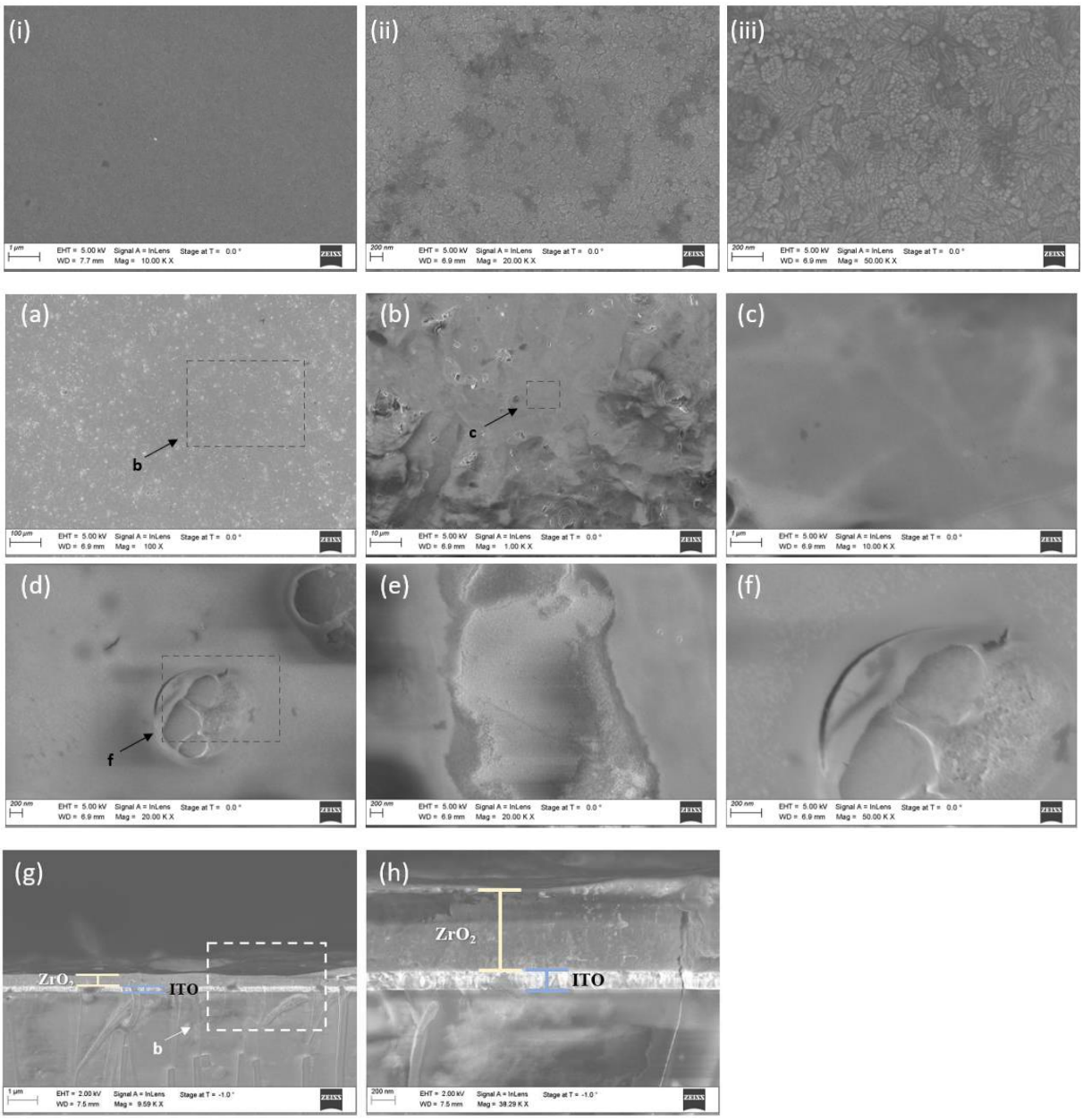

Figure 33: i)-iii) SEM micrographs of the glass/ITO substrate. a)-f) Plane-view and g)-h) cross-section SEM micrographs of ITO/ZrO_2 film deposited ZrO_2 at 410°C.

SEM micrographs for the **430°C** sample are presented in Fig. 34 and rings suggestive of droplet impact on the surface are observed. Upon magnification to the region b and c in Fig. 34 the deposits appear to be the borders or residuals of the droplets. Magnifying into regions that are located "within the droplets" indicate deposition of ZrO_2 (Fig. 34g). Regions of the surrounding deposit of the droplet borders (as magnified in Fig 34d and 34f) show grain structure that resembles more an ITO-like structure that is "covered with a veil of material".

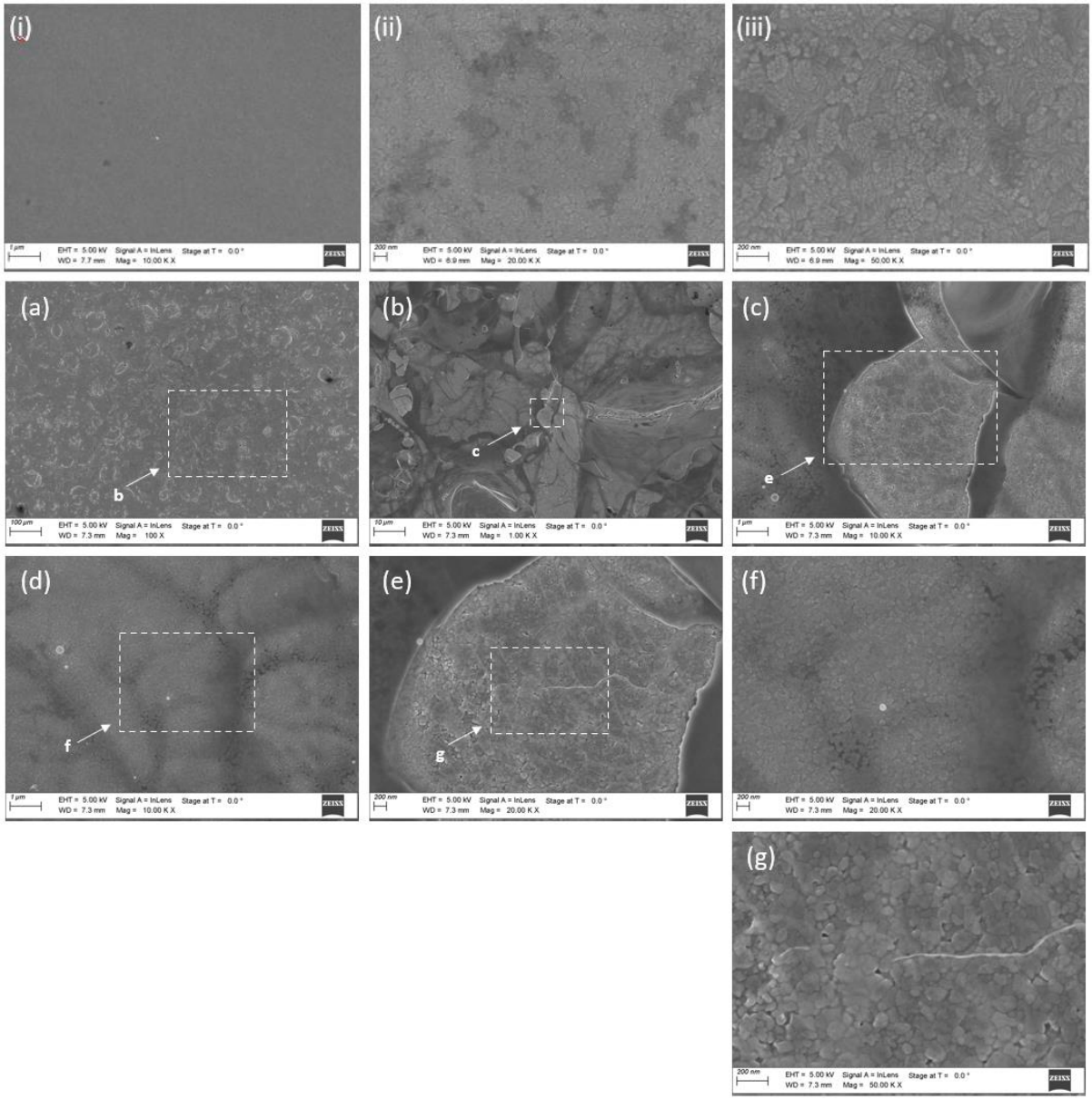

Figure 34: i)-iii) SEM micrographs of the glass/FTO substrate. a)-g) Plane-view SEM micrographs of FTO/ZrO_2 film deposited ZrO_2 at 430°C.

Conclusion and outlook

This thesis aimed to gain a better understanding of depositing stable ZrO_2 layers on transparent conducting oxide substrates while using spray pyrolysis from water-based precursor solutions. The chosen precursor salt was $ZrOCl_2 \times 8H_2O$, which is completely soluble in water and contributes to the acidic character of the solvent. The depositions were studied on three substrates: borosilicate glass, fluorine doped tin oxide and tin doped indium oxide. Despite the clear occurrence of cubic zirconium oxide on all layers, the process with the chosen parameters suffers from shortcomings that would have to be solved in the future. Three different experiment sets were conducted to analyse the concentration, scanning number repetition and temperature dependence of the chosen process.

While in theory for the working temperature (360°C – 430°C) formation of monoclinic ZrO_2 would be expected, in this work the cubic (111) texture was the most pronounced on all layers. For the experiment where the precursor solution concentration was varied, all diffraction peaks gained in intensity with increasing precursor concentration, which was caused by the increase of the thickness of the deposited ZrO_2 film. For the transparent conducting oxide substrates scanning electron microscopy has shown the impact of droplets as the solvent evaporated; the depositions seemed inhomogeneous in thickness according to cross-sectional micrographs an increase in thickness was observed on both FTO and ITO: While for the deposition created with the 25 mM precursor solution concentration a ~300 nm film was visible, with 50 mM layers of up to~800 - 1000 nm and (with 100 mM) >1.5 µm were observed. While the layers on ITO seemed more homogenous than the FTO, the observed film thicknesses were similar.
The scanning number repetitions were only analysed on borosilicate glass and ITO. For both samples the onset of crystallization was already visible at 75 scanning repetitions. Also evident was the increase of the reflection peaks' amplitude with increasing number of scans, which was the most pronounced for 250 scans.

The substrate temperature variation experiment was done between 360°C and 430°C on borosilicate glass and both TCO substrates. The film texture increased as the deposition temperature increased and was the highest for 410°C on all three substrates. With the SEM analysis subsequent growth from the liquid phase was observed. In some locations a grain structure that distinguishes itself from the one from the FTO/ITO substrate and from the surrounding deposit indicated grain growth from the vapour phase.

In this thesis, we have presented a series of experimental studies, which, we believe, have made the initial step to identify a successful route for the ZrO_2 deposition from $ZrOCl_2 \times 8H_2O$ as the precursor salt.

The question remains open, whether this process can be optimized to a route where nanocrystalline homogenous cubic ZrO_2 is formed on the chosen substrates. Although $ZrOCl_2 \times 8H_2O$ shows theoretically high potential in its function as a precursor salt, a few more experimental sets would have to be conducted in order to deposit a homogenous, nanocrystalline ZrO_2 layer. To gain more insight into the process, chosen salt and parameters, for example, testing the outcome of a deposition created with a lower concentration and higher scanning repetitions would be interesting or the addition of additives, such as PEG.[12]

Bibliography

1. Korotcenkov, G. Metal Oxides for Solid-State Gas Sensors: What Determines Our Choice? *Mater. Sci. Eng. B* **139**, 1–23 (2007).
2. Merdrignac, O. M., Moseley, P. T., Peat, R., Sofield, C. J. & Sugden, S. The modification of gas-sensing properties of semiconducting oxides by treatment with ionizing radiation. *Sensors Actuators B. Chem.* **7**, 651–655 (1992).
3. Moseley, P. T. Materials selection for semiconductor gas sensors. *Sensors Actuators B Chem.* **6**, 149–156 (1992).
4. Deshmukh, S. B. & Bari, R. H. Nanostructured ZrO_2 Thin Films Deposited by Spray Pyrolysis Techniques for Ammonia Gas Sensing Application. *Int. Lett. Chem. Phys. Astron.* **56**, 120–130 (2015).
5. Chen, C. Y., Tseng, T. K., Tsai, S. C., Lin, C. K. & Lin, H. M. Effect of precursor characteristics on zirconia and ceria particle morphology in spray pyrolysis. *Ceram. Int.* **34**, 409–416 (2008).
6. Králik, B., Chang, E. K. & Louie, S. G. Structural properties and quasiparticle band structure of zirconia. *Phys. Rev. B* **57**, 7027–7036 (1998).
7. Menzies, D. B., Cervini, R., Cheng, Y.-B., Simon, G. P. & Spiccia, L. Nanostructured ZrO2-Coated TiO2 Electrodes for Dye-Sensitised Solar Cells. *J. Sol-Gel Sci. Technol.* **32**, 363–366 (2004).
8. Nguyen, T. & Djurado, E. Deposition and characterization of nanocrystalline tetragonal zirconia films using electrostatic spray deposition. *Solid State Ionics* **138**, 191–197 (2001).
9. Wright, P. K. & Evans, A. G. Mechanisms governing the performance of thermal barrier coatings. *Curr. Opin. Solid State Mater. Sci.* **4**, 255–265 (1999).
10. Sun, J. *et al.* Room-Temperature-Processed ZrO2Interlayer toward Efficient Planar Perovskite Solar Cells. *ACS Appl. Energy Mater.* **3**, 3328–3336 (2020).
11. Oluwabi, A. T., Acik, I. O., Katerski, A., Mere, A. & Krunks, M. Structural and electrical characterisation of high-k ZrO2 thin films deposited by chemical spray pyrolysis method. *Thin Solid Films* **662**, 129–136 (2018).
12. Perednis, D. & Gauckler, L. J. Thin film deposition using spray pyrolysis. *J. Electroceramics* **14**, 103–111 (2005).
13. Perednis, D. & Gauckler, L. J. Solid oxide fuel cells with electrolytes prepared via spray pyrolysis. *Solid State Ionics* **166**, 229–239 (2004).
14. Markovic, J. P. *et al.* Nanostructured ZrO2 powder synthesized by ultrasonic spray pyrolysis. *Surf. Rev. Lett.* **14**, 915–919 (2007).
15. Ring, T. A. Ceramic Powder Synthesis. *Fundam. Ceram. Powder Process. Synth.* 81–83 (1996) doi:10.1016/b978-012588930-8/50004-8.
16. *Ceramic and Glass Materials*. *Ceramic and Glass Materials* (2008).
17. Blocher, J. M., Browning, M. F. & Barrett, D. M. Chemical Vapor Deposition of Ceramic Materials BT - Emergent Process Methods for High-Technology Ceramics. in (eds. Davis, R. F., Palmour, H. & Porter, R. L.) 299–316 (Springer US, 1984). doi:10.1007/978-1-4684-8205-8_23.
18. Spijksma, G. I., Blank, D. H. A., Bouwmeester, H. J. M. & Kessler, V. G. Modification of Different Zirconium Propoxide Precursors by Diethanolamine. Is There a Shelf Stability Issue for Sol-Gel Applications? *Int. J. Mol. Sci.* **10**, 4977–4989 (2009).
19. Kobayashi, J., Itaya, Y., Matsuda, H. & Hasatani, M. Drying Behaviour of ZrOCl2 Solution Droplet in ZrO2 Fine Particles Production by Spray Pyrolysis. *Bull. Polish Acad. Sci. Tech. Sci.* **Vol. 48**, **n**, 383–397 (2000).
20. Zhang, S. & Borden, M. Synthesis of. **67**, 61–67 (1990).
21. Muhammad, S. K. *et al.* Optical and Structural characterization of spraying ZrO2 and doped B: ZrO2 thin films. *J. Phys. Conf. Ser.* **1660**, (2020).
22. Martin, F., Ayouchi, R., Ruiz, C., Ramos-Barrado, J. R. & Leinen, D. Compositional and structural characterization of zirconia films with reticular structure obtained by spray pyrolysis. *Surf. Interface Anal.* **34**, 719–723 (2002).

23. Brog, J. P., Chanez, C. L., Crochet, A. & Fromm, K. M. Polymorphism, what it is and how to identify it: A systematic review. *RSC Adv.* **3**, 16905–16931 (2013).

24. Livraghi, S., Olivero, F., Paganini, M. C. & Giamello, E. Titanium Ions Dispersed into the ZrO2 Matrix: Spectroscopic Properties and Photoinduced Electron Transfer. *J. Phys. Chem. C* **114**, 18553–18558 (2010).

25. Wu, Y. *et al.* Phase transformation and oxygen vacancies in Pd/ZrO2 for complete methane oxidation under lean conditions. *J. Catal.* **377**, 565–576 (2019).

26. Emeline, A. V, Rudakova, A. V, Ryabchuk, V. K. & Serpone, N. Photostimulated Reactions at the Surface of Wide Band-Gap Metal Oxides (ZrO2 and TiO2): Interdependence of Rates of Reactions on Pressure−Concentration and on Light Intensity. *J. Phys. Chem. B* **102**, 10906–10916 (1998).

27. Gharibshahi, L., Saion, E., Gharibshahi, E., Shaari, A. H. & Matori, K. A. Structural and optical properties of ag nanoparticles synthesized by thermal treatment method. *Materials (Basel).* **10**, 402 (2017).

28. Xiaming, D., Qingfeng, L. & Yuying, T. Study of Phase Formation in Spray Pyrolysis of ZrO2 and ZrO2─;Y2O3 Powders. *J. Am. Ceram. Soc.* **76**, 760–762 (1993).

29. Kingery Bowen, H. Kent,, Uhlmann, D. R., W. D. *Introduction to ceramics*. (Wiley, 1976).

30. Bryant, W. A. The fundamentals of chemical vapour deposition. *J. Mater. Sci.* **12**, 1285–1306 (1977).

31. Ghoshtagore, R. N. Mechanism of {CVD} Thin Film {SnO}2 Formation. *J. Electrochem. Soc.* **125**, 110–117 (1978).

32. Suntola, T. Atomic layer epitaxy. *Thin Solid Films* **216**, 84–89 (1992).

33. Chamberlin, R. R. & Skarman, J. S. Chemical Spray Deposition Process for Inorganic Films. *J. Electrochem. Soc.* **113**, 86 (1966).

34. Brinker, C. J., Frye, G. C., Hurd, A. J. & Ashley, C. S. Fundamentals of sol-gel dip coating. *Thin Solid Films* **201**, 97–108 (1991).

35. Anderson, H. U., Nasrallah, M. M. & Chen, C.-C. Method of Coating a Substrate With a Metal Oxide Film From an Aqueous Solution Comprising a Metal Cation and a Polymerizable Organic Solvent. 1–25 (1996).

36. Balkenende, A. R., Bogaerts, A. A. M. B., Scholtz, J. J., Tijburg, R. R. M. & Willems, H. X. Thin MgO layers for effective hopping transport of electrons. *Philips J. Res.* **50**, 365–373 (1996).

37. Arya, S. P. S. & Hintermann, H. E. Growth of YBaCuO superconducting thin films by ultrasonic spray pyrolysis. *Thin Solid Films* **193**–**194**, 841–846 (1990).

38. Chen, C. H., Kelder, E. M., Jak, M. J. G. & Schoonman, J. Electrostatic spray deposition of thin layers of cathode materials for lithium battery. *Solid State Ionics* **86**–**88**, 1301–1306 (1996).

39. Filipovic, L. *et al.* Modeling spray pyrolysis deposition. *Lect. Notes Eng. Comput. Sci.* **2 LNECS**, 987–992 (2013).

40. Innovation by Design: What Makes Ultrasonic Nozzles Unique? https://www.sono-tek.com/ultrasonic-coating/how-ultrasonic-nozzles-work/ (last visited: 03/2022).

41. Lang, R. Ultrasonic Atomization of Liquid. *J. Acoust. Soc. Am.* **34**, 6 (1962).

42. Vigui, J. C. & Spitz, J. C h e m i c a l V a p o r Deposition a t Low T e m p e r a t u r e s Nozzte Furnace Qo Carrier gas Fogging system t ..... (. **268**, 2–5 (1971).

43. Cho, S. Y. *et al.* Effects of H2O2 on the morphology of ZrO2 powder prepared by ultrasonic spray pyrolysis. *Mater. Lett.* **32**, 271–273 (1997).

44. Habubi, N. F. *et al.* Effect of Cu doping ZrO2Thin films on physical properties grown by spray pyrolysis deposition. *IOP Conf. Ser. Earth Environ. Sci.* **790**, (2021).

45. García-Hipólito, M., Martínez, R., Alvarez-Fregoso, O., Martínez, E. & Falcony, C. Cathodoluminescent and photoluminescent properties of terbium doped ZrO2 films prepared by pneumatic spray pyrolysis technique. *J. Lumin.* **93**, 9–15 (2001).

46. Stelzer, N. H. J. & Schoonman, J. Synthesis of Terbia-doped Yttria-Stabilized Zirconia thin films by Electrostatic Spray Deposition (ESD). *J. Mater. Synth. Process.* **4**, 429–438 (1996).

47. Quan, Z. W., Wang, L. S. & Lin, J. Synthesis and characterization of spherical ZrO2:Eu 3+ phosphors by spray pyrolysis process. *Mater. Res. Bull.* **40**, 810–820 (2005).

48. Ramos-Brito, F., García-Hipólito, M., Alejo-Armenta, C., Alvarez-Fragoso, O. & Falcony, C. Characterization of luminescent praseodymium-doped ZrO 2 coatings deposited by ultrasonic spray pyrolysis technique. *J. Phys. D. Appl. Phys.* **40**, 6718–6724 (2007).

49. Perednis, D., Wilhelm, O., Pratsinis, S. E. & Gauckler, L. J. Morphology and deposition of thin yttria-stabilized zirconia films using spray pyrolysis. *Thin Solid Films* **474**, 84–95 (2005).

50. Arca, E., Fleischer, K. & Shvets, I. V. Influence of the Precursors and Chemical Composition of the Solution on the Properties of ZnO Thin Films Grown by Spray Pyrolysis. *J. Phys. Chem. C* **113**, 21074–21081 (2009).

51. Dataphyics. Surface tension values of some common test liquids for surface energy analysis Surface tension values of some common test liquids for surface energy analysis. **49**, 0–4 (2020).

52. Walther, C. *et al.* Investigation of polynuclear Zr(IV) hydroxide complexes by nanoelectrospray mass-spectrometry combined with XAFS. *Anal. Bioanal. Chem.* **388**, 409–431 (2007).

53. Ekberg, C., Källvenius, G., Albinsson, Y. & Brown, P. L. Studies on the Hydrolytic Behavior of Zirconium(IV). *J. Solution Chem.* **33**, 47–79 (2004).

54. Muha, G. M. & Vaughan, P. A. Structure of the complex ion in aqueous solutions of zirconyl and hafnyl oxyhalides. *J. Chem. Phys.* **33**, 194–199 (1960).

55. Mak, T. C. W. a Set of Scaled Structure Amplitudes Were Derived Using the. *Can. J. Chem.* **46**, 3491 (1968).

56. Martin, F., Lopez, M. C., Carrera, P., Ramos-Barrado, J. R. & Leinen, D. XPS depth profile study of porous zirconia films deposited on stainless steel by spray pyrolysis: The problem of substrate corrosion. *Surf. Interface Anal.* **36**, 8–16 (2004).

57. Peshev, P. *et al.* Spray pyrolysis deposition of nanostructured zirconia thin films. *Mater. Sci. Eng. B Solid-State Mater. Adv. Technol.* **97**, 106–110 (2003).

58. Wilkin, R. T., Wallschläger, D. & Ford, R. G. Speciation of arsenic in sulfidic waters. *Geochem. Trans.* **4**, 1–7 (2003).

59. COD - Database. http://www.crystallography.net/cod/ (last visited: 03/2022).

60. Liu, T., Zhang, X., Wang, X., Yu, J. & Li, L. A review of zirconia-based solid electrolytes. *Ionics (Kiel).* **22**, 2249–2262 (2016).

61. Pearce, E. M. Kirk-Othmer encyclopedia of chemical technology, 3rd ed., Vol. I, Wiley-Interscience, New York, 1978. *J. Polym. Sci. Polym. Lett. Ed.* **16**, 248 (1978).

Attachment

Zusammenfassung

In dieser Arbeit wurde der Fokus darauf gelegt, ein besseres Verständnis über die Deposition stabiler ZrO_2-Schichten auf transparenten leitfähigen Oxid-Substraten zu erlangen. Dafür wurden wasserbassierte Vorläuferlösungen mittels Sprühpyrolyse aufgetragen. Als Vorläufersalz wurde $ZrOCl_2 \times 8H_2O$ gewählt. Der Einfluss verschiedener Faktoren, die eine wichtige Rolle für den Sprühpyrolyseprozess spielen, wurde an drei Substraten untersucht: Borosilikatglas, fluordotiertes Zinnoxid (FTO) und zinndotiertes Indiumoxid (ITO). Die Konzentration der Vorläuferlösung wurde zwischen 25mM und 100mM variiert, um das Verhalten der ZrO_2-Schichten auf den gewählten Substraten zu untersuchen. Die Sprüh-wiederholungen wurden zwischen 75 und 250 gewählt, um die Entwicklung der Kristallisation mit zunehmender ZrO_2-Schichtdicke zu analysieren. Die Temperatur der Trägerplatte betrug 360°C bis 430°C, um die Auswirkungen auf den kristallinen Charakter der Schichten zu untersuchen. Die Kristallstruktur, die Morphologie und die Transmission der erhaltenen Schichten wurden mittels Rasterelektronenmikroskopie, Röntgenbeugung und Fourier-Transform-Spektroskopie untersucht.

Aufgrund von Unzulänglichkeiten war es nur teilweise möglich, kristalline ZrO_2-Schichten zu erhalten. Eine deutlich sichtbare Bildung von kubischem Zirkoniumdioxid konnte zwar auf allen Proben festgestellt werden, allerdings führte die Deposition unter den gewählten Bedingungen hauptsächlich zur Bildung von Tröpfchen. Eine weitere Optimierung des gewählten Prozesses und des Vorläufersalzes ist notwendig, um ein erfolgreiches Verfahren zur Herstellung einer homogenen Schicht zu erzielen. Diese könnte in weiteren Anwendungen wie Solarzellen oder optoelektronischen Produkten eingesetzt werden.